Neuron

Remyelination by surviving oligodendrocytes is inefficient in the inflamed mammalian cortex

Graphical abstract

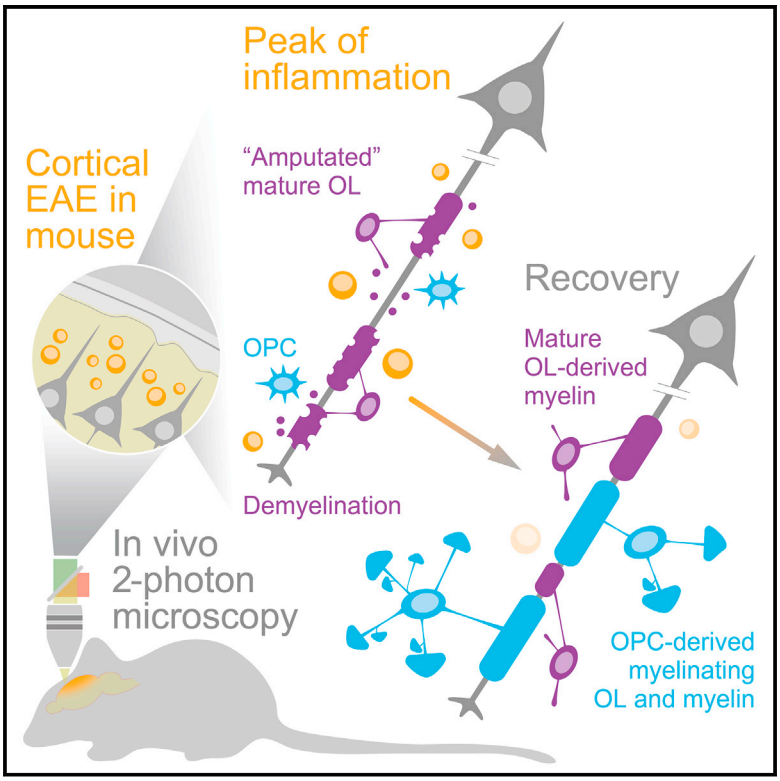

Highlights

- Surviving oligodendrocytes extend new proximal processes in the inflamed cortex
- However internode formation is rare and outweighed by ongoing internode loss
- Remyelination therapies do not boost the contribution of surviving oligodendrocytes

Authors

Aleksandra Mezydlo, Nils Treiber, Emily Melisa Ullrich Gavilanes, ..., Nicolas Snaidero, Thomas Misgeld, Martin Kerschensteiner

Correspondence

thomas.misgeld@tum.de (T.M.), martin.kerschensteiner@med.uni-muenchen.de (M.K.)

In brief

Meyzdlo et al. study whether surviving oligodendrocytes contribute to myelin recovery in a multiple sclerosis model. They show that these cells attempt but often fail to remyelinate. Drugs that promote myelin formation by oligodendrocyte precursor cells do not affect surviving oligodendrocytes, indicating that surviving oligodendrocytes require distinct therapeutic targeting.

Mezydlo et al., 2023, Neuron *111*, 1748–1759
June 7, 2023
https://doi.org/10.1016/j.neuron.2023.03.031

CellPress

CellPress

Neuron

Report

Remyelination by surviving oligodendrocytes is inefficient in the inflamed mammalian cortex

Aleksandra Mezydlo,[1,2,3,8] Nils Treiber,[1,2,8] Emily Melisa Ullrich Gavilanes,[1,2] Katharina Eichenseer,[3,4] Mihai Ancău,[3,5] Adinda Wens,[1,2] Carla Ares Carral,[1,2] Martina Schifferer,[3,6,7] Nicolas Snaidero,[3,4] Thomas Misgeld,[3,6,7,9,*] and Martin Kerschensteiner[1,2,7,9,10,*]

[1]Institute of Clinical Neuroimmunology, University Hospital, Ludwig-Maximilians Universität München, Munich, Germany
[2]Biomedical Center (BMC), Faculty of Medicine, Ludwig-Maximilians Universität München, Martinsried, Germany
[3]Institute of Neuronal Cell Biology, Technical University of Munich, Munich, Germany
[4]Hertie Institute for Clinical Brain Research, Tübingen, Germany
[5]Department of Neurology, Klinikum Rechts der Isar, Technical University of Munich, Munich, Germany
[6]German Center for Neurodegenerative Diseases (DZNE), Munich, Germany
[7]Munich Cluster for Systems Neurology (SyNergy), Munich, Germany
[8]These authors contributed equally
[9]Senior author
[10]Lead contact
*Correspondence: thomas.misgeld@tum.de (T.M.), martin.kerschensteiner@med.uni-muenchen.de (M.K.)
https://doi.org/10.1016/j.neuron.2023.03.031

SUMMARY

In multiple sclerosis, an inflammatory attack results in myelin loss, which can be partially reversed by remyelination. Recent studies suggest that mature oligodendrocytes could contribute to remyelination by generating new myelin. Here, we show that in a mouse model of cortical multiple sclerosis pathology, surviving oligodendrocytes can indeed extend new proximal processes but rarely generate new myelin internodes. Furthermore, drugs that boost myelin recovery by targeting oligodendrocyte precursor cells did not enhance this alternate mode of myelin regeneration. These data indicate that the contribution of surviving oligodendrocytes to myelin recovery in the inflamed mammalian CNS is minor and inhibited by distinct remyelination brakes.

INTRODUCTION

Remyelination is one of few endogenous repair processes in the mammalian CNS. Still, this process often fails. For example, in multiple sclerosis (MS), a common demyelinating CNS disease, remyelination can be detected in some patients but is inefficient in most.[1–3] Therefore, defining which cells promote remyelination is central to unraveling MS pathogenesis and devising restorative CNS therapies.

For a long time, the notion prevailed that remyelination depends on the differentiation of oligodendrocyte precursor cells (OPCs), which would thus be the sole source of new myelin.[4] However, recent studies have challenged this dogma and suggest that surviving oligodendrocytes make a substantial contribution to remyelination by growing new internodes even in the mature mammalian CNS.[5–9] However, although we previously described surviving oligodendrocytes in neuroinflammatory lesions—some in an "amputated" state without internodes but preserved proximal processes[10]—it remains unclear whether internode formation from mature oligodendrocytes is efficient,[11] amendable to current remyelination therapies,[9] and quantitatively relevant to remyelination in the inflammatory milieu of MS lesions.[12,13]

We tackled this question in a recently established mouse model of cortical MS (c-MS) [14] because cortical demyelination is linked to clinical progression in MS and thus an important therapeutic target.[1,2,15] Furthermore, the sparsity of oligodendrocytes in gray matter allows long-term tracking of myelination patterns with cellular resolution.[16–18] We established a conditional genetics approach that resulted in the fluorescent tagging of individual surviving oligodendrocytes and used *in vivo* microscopy to follow their fate over a cycle of inflammatory de- and remyelination. Our results show that although surviving oligodendrocytes can form new proximal processes during cortical remyelination, internode re-formation is so infrequent that even during the recovery phase it is typically outweighed by simultaneous internode loss. Notably, treatment with the remyelination-promoting drugs clemastine[19] and metformin[20] boosted myelin recovery without any contribution from surviving oligodendrocytes. Taken together, our results show that while damaged oligodendrocytes can survive long term in the inflamed CNS and show abortive signs of regeneration, they ultimately fail to make a consequential contribution to myelin recovery.

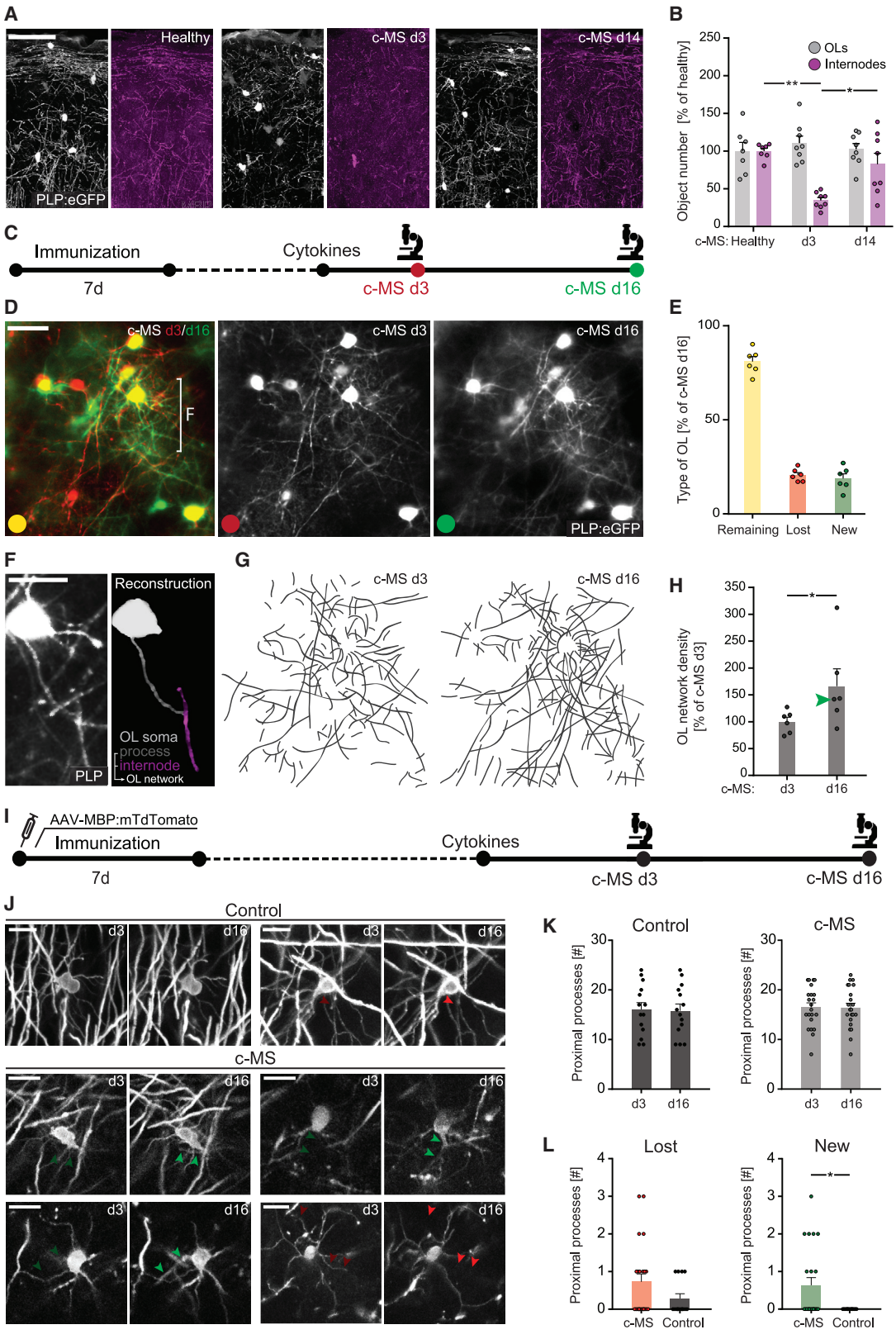

(legend on next page)

RESULTS

Many oligodendrocytes survive demyelination in a cortical MS model

To study the fate of myelin and oligodendrocytes in the inflamed gray matter, we first characterized the time course of demyelination and remyelination in our c-MS model[14] using proteolipid protein (PLP):EGFP mice, where oligodendrocytes are fluorescently labeled.[21] Histopathology revealed widespread subpial demyelination akin to the pattern observed in human MS.[22] Loss of internodes was extensive 3 days after cortical lesion induction (c-MS day 3) but mostly recovered 11 days later (c-MS day 14), whereas the density of PLP:EGFP expressing cells remained unchanged (Figures 1A, 1B, and S1). Given the homeostatic replacement of damaged oligodendrocytes observed previously in the non-inflamed mouse cortex,[18,23] we explored whether similar dynamic turnover maintains oligodendrocyte density in c-MS. Time-lapse *in vivo* imaging revealed that about a fifth of mature oligodendrocytes are replaced between day 3 and 16 of c-MS, but overall oligodendrocyte numbers were stable (Figures 1C–1E). Notably, in parallel, there was an increase in the density of the oligodendrocyte "network" that includes processes from the soma and their terminal internodes (Figures 1F–1H). This raises the question of whether the ~80% surviving oligodendrocytes in our c-MS model can contribute to myelin recovery as recently suggested.[5–9]

Surviving oligodendrocytes can extend new processes

To explore this question, we established a viral labeling strategy that resulted in sparse labeling of oligodendrocytes (Figure S2A; see STAR Methods for details). *In vivo* imaging revealed that surviving oligodendrocytes can indeed extend new proximal processes during the remyelination phase (between c-MS day 3 and 16). However, these cells continue to lose processes during the same time so that the overall number of proximal processes per surviving oligodendrocyte remained unchanged (Figures 1I–1L).

In the context of remyelination, the critical question is whether the surviving oligodendrocytes can also form new internodes. Indeed, time-lapse imaging revealed the profuse formation of new internodes in the immediate vicinity of damaged oligodendrocytes. However, we noted that the addition of new internodes was often associated with the local emergence of newly differentiated oligodendrocytes, which tended to be faintly labeled (Figures 2A and 2B). Thus, to establish that newly formed internodes indeed traced back to surviving oligodendrocytes, we used correlative light-to-electron microscopy (CLEM). Notably, our analysis revealed that 3 out of 8 primary processes of the surviving oligodendrocyte that we reconstructed crossed within a distance typically not resolvable by *in vivo* imaging of either a process or an internode formed by the newly differentiated cell (Figure 2C; Video S1). This argues that a more refined labeling approach is required to unambiguously assess the remyelination contribution of newly differentiated vs. surviving oligodendrocytes.

Newly differentiating oligodendrocytes efficiently remyelinate inflamed mouse cortex

We first selectively labeled newly formed oligodendrocytes using tamoxifen/CreER-mediated lineage tracing in an NG2:CreER^{T2} mouse line[24] crossed to a ubiquitous CAG-CAT-EGFP reporter strain.[25] After intraperitoneal (i.p.) tamoxifen injection and c-MS induction (Figure 2D), this approach resulted in two-photon microscopy compatible labeling of cells showing an OPC-like ramified morphology (Figure 2E). In c-MS lesions, such cells over time differentiated and extended T-shaped elaborations, which spectral confocal reflectance microscopy (SCoRe) imaging[26] and myelin basic protein (MBP) staining confirmed to be internodes (Figures 2E and S2B). Notably, the number of such GFP+ cells with an oligodendrocyte-like morphology rose steeply until c-MS day 25 (Figures 2F and 2G). This was accompanied by the steady addition of laterally expanding internodes (Figures 2H–2J), suggesting remyelination as shown previously using similar techniques,[27] in line with the view that a substantial part of remyelination in inflamed mouse cortex is dependent on newly differentiating oligodendrocytes.

Internode formation by surviving oligodendrocytes is inefficient

Next, we used a similar approach to label surviving oligodendrocytes in inflammatory lesions. For this purpose, we injected an

Figure 1. Myelin loss, oligodendrocyte turnover, and process formation in the c-MS model

(A) Confocal images of oligodendrocytes (OL, GFP, gray) and internodes (MBP, magenta) in PLP:EGFPxBiozziABH somatosensory cortex (300 μm lateral to the injection site). Left: healthy control; middle: c-MS day (d) 3; right: c-MS day 14.

(B) OL number and internode density at c-MS day 3 (n = 8 mice), c-MS day 14 (n = 8) normalized to healthy control (n = 7).

(C) Timeline of the *in vivo* experiment to measure OL turnover.

(D) Projections of two-photon image stacks of the top 60 μm of inflamed layer 1 in a PLP:EGFPxBiozziABH somatosensory cortex. c-MS day 3 (middle, red) and day 16 (right, green). In the overlay (left), remaining, lost, and new OLs appear yellow, red, and green, respectively.

(E) Quantification of remaining, lost, and new OLs at c-MS day 16 compared with day 3.

(F) Partial projection of a GFP-labeled OL at higher magnification (area marked by the bracket in D). Left: projection of the two-photon stack; right: surface rendering, with OL soma (white), a primary process (gray), and an internode (magenta).

(G) Tracing of GFP+ processes and internodes ("OL network") in the same area over the course of c-MS.

(H) OL network density within c-MS lesions at day 16 normalized to day 3 (n = 6 mice, 3–7 areas/mouse); green arrowhead points to data point illustrated in (G).

(I) Experimental design to investigate dynamics of mature OLs in cortical c-MS lesions.

(J) High magnification images of mTdTomato+ OLs and their proximal processes at day 3 and 16 in control (non-immunized animals, top) and in c-MS (middle and bottom). Red arrowheads, lost processes; green arrowheads, new processes.

(K and L) Quantification of the total number of proximal processes (K) and of lost and new proximal processes (L) during the course of c-MS (c-MS, n = 22 OLs/6 mice; controls n = 14/5).

Scale bars, 100 μm (A), 50 μm (D), 20 μm (F and J). Data show mean ± SEM. Kruskal-Wallis followed by Dunn's multiple comparisons test has been performed in (B), Mann-Whitney test in (H), (L), and t test in (K). $^{**}p < 0.01$, $^{*}p < 0.05$. See also Figure S1.

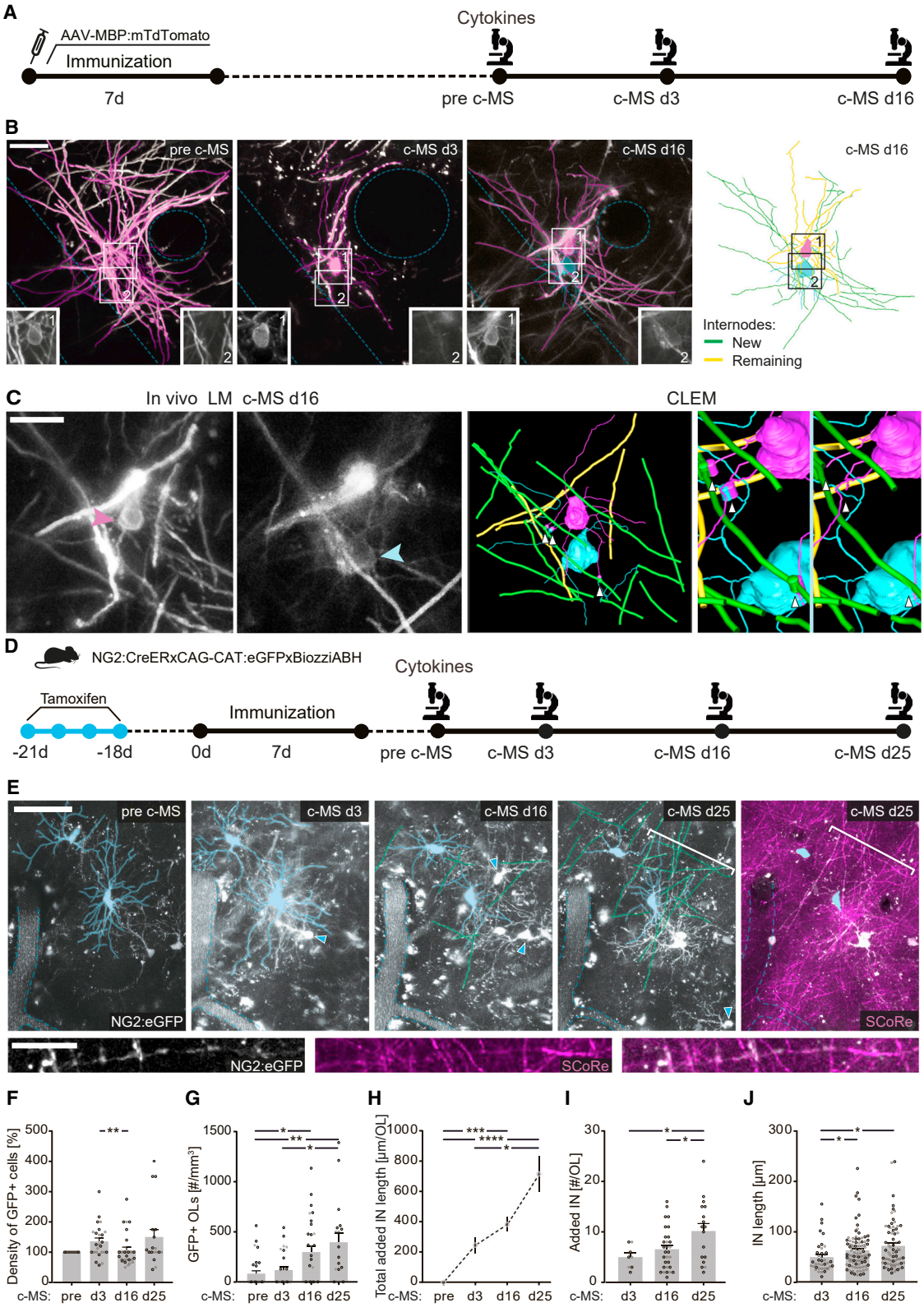

(legend on next page)

AAV-MBP:CreER^{T2} virus into the cortex of ROSA:mT/mG reporter mice.[28] Tamoxifen treatment several weeks before induction of the c-MS model resulted in sparse and selective labeling of mature oligodendrocytes in the injected cortex areas (Figures 3A, 3B, and S3A). With this labeling, *in vivo* time-lapse imaging allowed the tracking of regressive and regenerative events specifically in mature oligodendrocytes during a de-/remyelination cycle. Our results showed a pronounced loss of internodes up to c-MS day 3, with both reductions in internode number and length (Figures 3C–3E). During the early (c-MS day 3–16) and later (up to day 25) remyelination phase we indeed observed some regenerative events originating from preexisting oligodendrocytes, including the formation of internodes and the extension of preexisting internodes (Figure 3B). However, these events were rare and, even in the same cells, were outweighed by ongoing internode loss (Figures 3C–3F). Altogether, these restorative processes on average only led to the gain of about 8 % of the original myelin length up to c-MS day 25 (Figure 3F), with the prevailing mode of remyelination being the restoration of internodes on axons that had originally been demyelinated (Figure 3G). Although such cases of restorative internode formation were rare, if they happened, they often replaced a substantial fraction of the previously lost internode (Figure 3H). Both regressive and regenerative changes in surviving oligodendrocytes appeared to be influenced by the extent of damage the cell suffered over the initial demyelination phase (Figures S3B–S3F). Notably, even severely damaged oligodendrocytes mostly survived at least up to day 25 after c-MS induction (Figure S3G). Sometimes myelin extended by surviving oligodendrocytes transiently showed abnormal morphologies, such as local swellings (Figure S3H), but counter to what has been reported in larval zebrafish after chemogenetic oligodendrocyte injury,[11] we did not observe that surviving oligodendrocytes wrapped cell bodies in the upper cortical layers (n = 223 surviving oligodendrocytes from 6 mice, during the remyelination phase of c-MS), a morphology that overall was rarely observed in c-MS cortex (Figure S4; 0.09 ± 0.04 myelin-wrapped neurons/mm^2 cortex; 3 wrapped neuronal somata among 116.110 neurons; n = 6 mice and 60 cortical sections, analyzed during the remyelination phase of c-MS).

Surviving oligodendrocytes are also not major contributors to remyelination following other forms of myelin damage

To explore, whether the inefficient contribution of surviving oligodendrocytes to cortical remyelination was a specific feature of the neuroinflammatory milieu of c-MS, we turned to two further models of cortical oligodendrocyte injury. First, we combined the AAV-MBP:CreER^{T2}/ROSA:mT/mG-based labeling of mature oligodendrocytes with a two-photon laser ablation paradigm that we recently introduced[18] in which a small number (1–3) of oligodendrocyte somata were ablated without causing discernible damage to the surrounding (Figure 4A). Within about one month, most of the myelin sheaths supported by the ablated cells were cleared (Figures 4B and 4C), and efficient remyelination ensued as described previously.[18] In this setting, we observed neither internode restoration nor substantial net internode extension into the demyelinated territory originating from the uninjured surrounding oligodendrocytes (Figure 4D). This suggests that in a "sterile" setting, where oligodendrocytes are either lethally injured or intact, the homeostatic replacement of myelin sheaths is entirely mediated by newly differentiating oligodendrocytes.[18] Next, we used a recombinant antibody against myelin oligodendrocyte glycoprotein (MOG-IgG) and human complement to target labeled mature oligodendrocytes (Figure 4E), which models a humoral autoimmune reaction that relates to myelin oligodendrocyte glycoprotein antibody-associated disease (MOGAD[29]). Here, we observed swift and broad demyelination with partial oligodendrocyte loss, but again no signs of internode formation by the labeled oligodendrocytes (Figure 4F). Thus, neither in the pro-inflammatory milieu of c-MS,[14] nor in antibody/complement-induced lesions or in a nearly undamaged neuropil do mature oligodendrocytes play a substantial role in restoring myelin (Figure 4G).

Figure 2. New oligodendrocytes differentiate and form myelin internodes in the immediate vicinity of damaged oligodendrocytes

(A) Experimental design to investigate dynamics of mature OLs in cortical c-MS lesions.

(B) Left, a mTdTomato+ OL tracked over time. Reconstructed processes and internodes (magenta) overlaid on the mTdTomato signal. Insets show surviving OL soma (1) and newly differentiated OL (2) at c-MS day 16. Right, 3-D reconstruction of processes and internodes at c-MS day 16; remaining structures, connected to the surviving OL are marked in yellow, new structures are marked in green.

(C) CLEM 3D reconstructions of surviving OL and newly differentiated OL with their respective processes (corresponding time-lapse shown in B). Left two images show two frames of two-photon stacks, spaced by 9 μm (magenta arrowhead, surviving OL; cyan arrowhead, newly differentiated OL). The right images show 3D renderings of the surviving (magenta) and newly differentiated (cyan) OL and their processes as well as new (green) and remaining (yellow) myelin internodes. Higher magnification of the 3D reconstruction with and without cylinders representing the approximate size of the point spread function illustrates three sites (white arrowheads) at which processes cross other processes or internodes within the diffraction limit.

(D) Experimental design to investigate newly differentiating OLs in the c-MS model.

(E) *In vivo* time-lapse images illustrating internode formation (marked in green) by newly differentiating cells (cyan) starting at c-MS day 16 and confirmed by SCoRe imaging at c-MS day 25. GFP+ cells that newly appear during the time-lapse are marked by cyan arrowheads. An example of a newly formed SCoRe+ internode (bracketed in E) is shown in higher magnification in the insets below.

(F and G) Quantification of the density of all GFP+ cells (F, values normalized to pre-c-MS time point per imaged area) and number of GFP+ OLs (G) per imaged area (n = 29 areas analyzed from 6 mice, of which 19 areas from 3 mice were imaged until day 25).

(H and I) Total added internode length (H) and number of added internodes (I) per newly differentiating GFP+ OL (for definition see STAR Methods; n = 7 mice, 8 cells at c-MS day 3, 30 cells at c-MS day 16 and 17 cells at c-MS day 25).

(J) Length of individual internodes originating from differentiating GFP+ OLs (n = 7 mice, 40 internodes at c-MS day 3, 95 internodes at c-MS day 16, and 71 internodes at c-MS day 25).

Scale bars, 50 μm (B and E), 20 μm (C and E inset), Data shown as mean ± SEM. Kruskal-Wallis followed by Dunn's multiple comparisons test in (F), (G), (I), and (J). One-way ANOVA followed by Tukey's multiple comparison test in (H). ****p < 0.0001, ***p < 0.001, **p < 0.01, *p < 0.05. See also Figure S2.

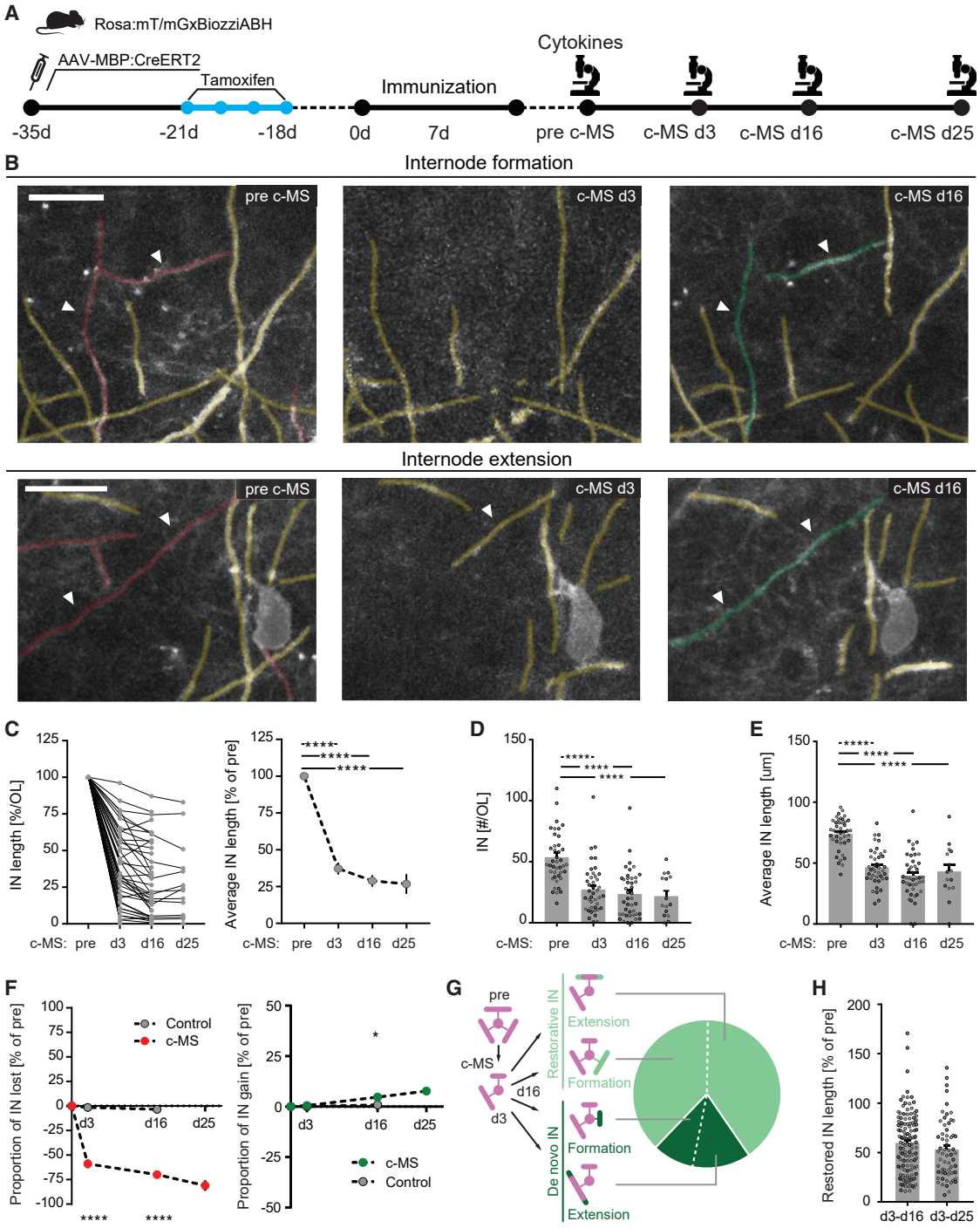

Figure 3. Internode formation by surviving oligodendrocytes in the c-MS model is inefficient and does not compensate for ongoing internode loss

(A) Schematic of *in vivo* imaging of internode formation by selectively tagged surviving OLs in c-MS.

(B) High-magnification time-lapse projections of two-photon imaging stacks from c-MS lesions (shown with semi-automated tracing and fate assignment) illustrating recovery modes by surviving mGFP+ OL. Remaining (yellow), lost (red), and new or extended (green) internodes are pseudo-colored, and arrowheads indicate restored myelin segments.

(C) Quantification of internode length changes in surviving OLs at single cell (left, per area, 1-6OLs) and at the population level (right) during the course of c-MS lesion formation and recovery.

(legend continued on next page)

Surviving oligodendrocytes in c-MS are refractory to clemastine/metformin therapy

Finally, we explored whether therapies that promote myelin formation in the inflamed CNS can recruit surviving oligodendrocytes to the remyelination process. We again injected an AAV-MBP:CreER virus into the cortex of ROSA:mT/mG reporter mice and treated these mice between c-MS day 3 and 16 with a combination of clemastine and metformin (Figure 4H), both drugs that have been shown to improve remyelination.[19,20] Indeed, treatment with clemastine/metformin did increase myelin density in the cortex by about 50% at c-MS day 16 (Figure 4I). However, time-lapse recordings revealed that myelin restoration was achieved without any contribution of surviving oligodendrocytes, which continued to lose internodes between c-MS day 3 and day 16 in the absence of any regenerative changes (Figures 4J and 4K). This indicates that therapies that support remyelination via OPCs do not also support and might even limit myelin formation by surviving oligodendrocytes, at least in the cortex.

DISCUSSION

The cellular and molecular mechanisms of remyelination in the inflamed CNS are central to our understanding of MS pathology and to the design of therapeutic strategies to support CNS restoration, even beyond MS.[30] One of the fundamental unresolved questions is, which cell populations can contribute to myelin repair and should thus be targeted. Although the classical concept stipulates that myelin repair requires *de novo* differentiation of new oligodendrocytes from OPCs,[4,31] recent studies suggest that mature oligodendrocytes contribute substantially to myelin repair.[5–9]

As remyelination capacity is highly dependent on the local microenvironment and injury type,[4,9,32] we wanted to resolve the contribution of mature oligodendrocytes to myelin repair in a model that mimics c-MS pathology.[14,33,34] Here, we observe that despite the extensive loss of myelin in these lesions, about 80% of mature oligodendrocytes survive. This indicates that most mature oligodendrocytes can persist despite extensive damage to their process and internode network, reminiscent of the amputated state of "demyelinated oligodendrocytes" that was previously described in MS[35] and in inflammatory white matter lesions in mice.[10] Although oligodendrocytes thus mostly survive, we observed rapid myelin damage that is initiated within three days after lesion induction and is followed by similarly swift induction of myelin repair leading to substantial myelin recovery within two weeks. The propensity of cortical lesions to remyelinate is reminiscent of findings in MS patients[36,37] and could be related to the less pronounced axon damage present in both human and experimental gray matter lesions compared with white matter lesions.[14,38]

The survival of axonal targets for myelination, as well as mature "demyelinated" oligodendrocytes in a highly inflammatory environment thus makes the c-MS model a suitable paradigm to study the contribution of surviving oligodendrocytes to the remyelination process in neuroinflammatory lesions, especially as these lesions are easily accessible for long-term *in vivo* imaging. However, our experiments revealed that two-photon microscopy alone is insufficient to demonstrate that surviving oligodendrocytes form new myelin sheaths due to the swift emergence of new oligodendrocytes in the immediate vicinity of surviving oligodendrocytes.[18] Indeed, our CLEM analysis demonstrated that it is often not possible to unambiguously trace oligodendrocyte processes to the newly formed myelin internodes and several instances of ambiguity ensue even in a single pair of cells. We thus established a "lineage-tracing" approach that indelibly labels mature oligodendrocytes, which survived in c-MS lesions and revealed that these cells contribute little to remyelination, as they rarely formed new internodes, and even if they did, this new myelin formation was outweighed by continued internode loss. Similarly, surviving oligodendrocytes seem to make at best a minor contribution to remyelination in other models of oligodendrocyte injury, such as laser ablation or antibody/complement-mediated injury. Thus, at least in the adult mouse cortex, new oligodendrocytes are responsible for the bulk of endogenous remyelination. Indeed, the direct observation of efficient and ongoing remyelination, when transferring the lineage-tracing approach to OPCs directly corroborated this notion. Whether the cells that mediate remyelination invariably derived from proliferating OPCs or rather from more differentiated precursors,[39] such as pre-myelinating BCAS-expressing cells,[40] remains unresolved, but the fact that internode formation of newly differentiating oligodendrocytes starts early (at day 3 after cytokine injection) seems compatible with a pre-differentiated "cell-in-waiting" that accelerated cortical remyelination.

By tracking single internodes in sparsely lineage-labeled oligodendrocytes, we found that the few internodes produced by surviving oligodendrocytes mostly restored previously demyelinated segments, in line with previous observations by others and us that specific cortical axons are especially targeted for remyelination.[18,41] Likewise in the c-MS model, we

(D and E) Quantification of the evolution of the internode number (D) and length (E) per OL in the c-MS model. For (C–E), 42 areas (1–6 OL/area) from 16 mice were imaged up to c-MS day 16. Of these 15 areas, 7 mice were imaged up to c-MS day 25. For (E), per area, the length of 25–270 internodes was averaged (1–6 OLs/area).

(F) Quantification of the total length of lost (left) and new or extended internodes (right) in surviving OLs in the c-MS model vs. non-immunized, cytokine-injected controls; in % related to the total internode length of the OL before lesion induction; c-MS (n = 16 mice, 42 areas imaged up to day 16 of which 15 areas from 7 mice were followed up to c-MS day 25; 1–6 OLs/area), controls (n = 4 mice and 9 areas imaged up to day 16; 1–4 OLs/area).

(G) Schematic and pie chart illustrating the mechanisms that contribute to new myelin formation by surviving OLs at c-MS day 16 (all extended or newly formed internodes were included in the analysis, see STAR Methods for definition; n = 435 internodes).

(H) Quantification of the extent of restorative internode formation at c-MS day 16 and c-MS day 25 (in % of the initial internode length before c-MS induction; all newly formed internodes that restored lost internodes were included in the analysis; n = 123 internodes at c-MS day 16 and 61 internodes at c-MS day 25).

Scale bars, 20 μm (B) Data shown as mean ± SEM. Kruskal-Wallis followed by Dunn's multiple comparisons test has been performed in (C) and Mann-Whitney test was used for each time point in (D), (E), (F), and (G). ****$p < 0.0001$, *$p < 0.05$. See also Figures S3 and S4.

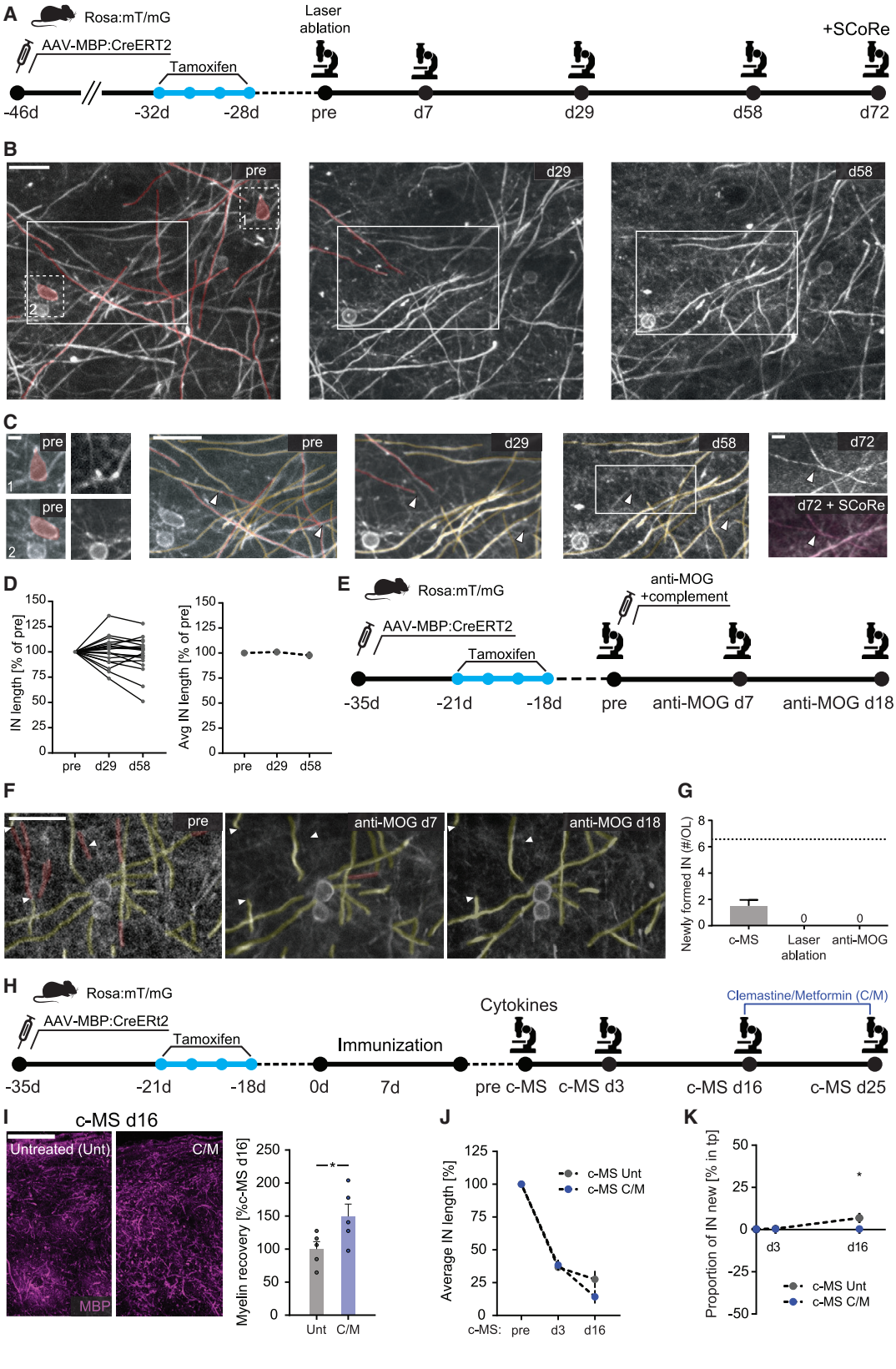

(legend on next page)

only rarely observed evidence for myelin mistargeting such as neuronal cell body wrapping.[11] Here, it is to be noted that our *in vivo* observations strictly only apply to the superficial layers of mouse cortex, where both the composition of the axon populations, as well as the local oligodendrocyte lineage might show specific features, resulting in layer-specific regulation of remyelination.[13] Still, as now data from phylo- and ontogenetically distant zebrafish larvae[11] and from adult mammalian cortex concur regarding the low efficacy of mature oligodendrocytes in forming proper myelin, the old dogma of OPC-primacy in remyelination should perhaps not be abandoned quite yet.[4] This is not only significant for MS research but also warrants consideration in the context of CNS repair strategies, where myelination is needed in an environment without primary demyelination.[42,43]

At the same time, the fact that surviving oligodendrocytes clearly initiate a regenerative—albeit abortive—response, with the formation of new primary processes and occasionally new internodes, implies that such cells could still be viable targets for remyelination therapies. As most remyelination therapies to date were developed with a focus on OPCs[1,2,4] a critical question is whether such OPC-targeted therapies can also enhance the contribution of surviving oligodendrocytes. We focused our analysis on one of the most promising and clinically advanced approaches to support OPC-derived myelination, combined clemastine/metformin treatment. Although this therapy indeed improved overall myelin recovery, it did not enhance remyelination by surviving oligodendrocytes. On the contrary, it even suppressed the abortive regenerative attempts that we observed in untreated mice, either because the drugs directly interfere with the growth response in mature oligodendrocytes or more likely because OPCs and surviving oligodendrocytes compete for suitable myelination targets. Thus, surviving oligodendrocytes at best represent a distinct target for therapy from OPCs, but perhaps even a competing one that needs to be targeted by tailored pharmacological interventions. This opens the possibility for the design of novel remyelination concepts and therapies that aim to recruit surviving oligodendrocytes to the myelin repair process.

STAR★METHODS

Detailed methods are provided in the online version of this paper and include the following:

- KEY RESOURCES TABLE
- RESOURCE AVAILABILITY
  - Lead contact
  - Materials availability
  - Data and code availability
- EXPERIMENTAL MODEL AND SUBJECT DETAILS
- METHOD DETAILS
  - Induction of the cortical MS model (c-MS model)
  - Induction of the cortical anti-MOG model
  - Laser ablation of cortical oligodendrocytes
  - Immunofluorescence staining
  - Confocal microscopy
  - AAV vector generation and virus production
  - Single-cell labeling of individual oligodendrocytes
  - Cranial window surgery
  - *In vivo* imaging
  - Correlative light-to-electron microscopy (CLEM)

Figure 4. Surviving oligodendrocytes do neither remyelinate following laser- and antibody-mediated demyelination nor respond to clemastine/metformin therapy

(A) Schematic of *in vivo* imaging experiment to follow the response of mature OLs to laser ablation of neighbors.

(B) Projections of multi-photon imaging stacks from a ROSA:mT/mG mouse cortex in which mature OLs are fluorescently labeled (white) before ("pre") and at day 29 and 58 after laser ablation (ablated cells are shown in red in the left panel). Images are shown with semi-automated tracing and fate assignment (internodes that were lost by the next time point are shown in red).

(C) Insets on the left illustrate the loss of laser ablated cells ("1" and "2") after 7 days. Larger panels show the area boxed in (B) over the course of the ablation experiment (lost internodes are colored in red, stable internodes in yellow). The arrowheads mark the nodes of a segment of interest lost after laser ablation. On the right, the magnification of the box at day 58 shows this region on day 72, and below, the same image is overlaid by a SCoRe image (magenta), illustrating the remyelination of the previously lost segment.

(D) Quantification of the individual and average length changes of internodes derived from mature OLs that are neighboring the demyelinated segments over time (n = 20 internodes derived from 4 areas, in which 1-3OLs were ablated).

(E) Schematic of *in vivo* imaging experiment to follow the response of surviving OLs following antibody-mediated demyelination.

(F) Projections of two-photon imaging stacks from a ROSA:mT/mG mouse cortex in which mature OLs are fluorescently labeled (white) before (pre) and at day 7 (anti-MOG day 7) and day 18 (anti-MOG day 18) after induction of the cortical demyelination. Internode fates are pseudo-colored as above.

(G) Quantification of internode formation by mature OLs in the c-MS model (c-MS day16; n = 42 areas with 86 OLs analyzed), anti-MOG model (anti-MOG day 18; n = 43 OLs analyzed), and after laser ablation of cortical OLs (day 58; after laser ablation of OLs with 214 myelin internodes, n = 16 neighboring OLs analyzed). The dashed line shows internode formation by newly differentiating OLs at c-MS day 16 for comparison (cf. Figure 2I).

(H) Schematic of *in vivo* imaging experiments to determine the response of surviving oligodendrocytes to clemastine/metformin ("C/M") therapy in the c-MS model.

(I) Confocal images (left panels) and quantitative immunohistochemical analysis of myelin density (MBP staining, magenta) in mice treated with clemastine/metformin compared with untreated ("unt") controls (n = 5).

(J) Quantification of internode length changes in surviving OLs during the course of c-MS in clemastine/metformin-treated mice (n = 3 mice, 4 areas, 1-2OLs/area) compared with surviving OLs with similar initial damage at c-MS day 3 in untreated mice (n = 4/7/1–3; a subset of the data shown in Figure 3C).

(K) Quantification of the total length of new and extended internodes in surviving OLs in % related to the OL size before lesion induction (pre) in c-MS mice treated with clemastine/metformin (n = 4 mice, 5 areas, 1-2OLs/area) compared with surviving OLs with similar initial damage at c-MS day 3 in untreated mice (n = 4/7/1–3; a subset of the data shown in Figures 3C–3F).

Scale bars, 20 μm in (B) and (C, large panel), 5 μm in (C, small panels on the left and right), 20 μm in (F), and 100 μm (I). Data shown as mean ± SEM. Mann-Whitney test was used for each time point in (I), (J), and (K). *$p < 0.05$.

SUPPLEMENTAL INFORMATION

Supplemental information can be found online at https://doi.org/10.1016/j.neuron.2023.03.031.

ACKNOWLEDGMENTS

We thank A. Schmalz, J. Schmitt, B. Fiedler, and Y. Hufnagel for excellent technical assistance and D. Matzek, B. Stahr, M. Korica, N., and M. Budak for animal husbandry. PLP-EGFP mice[21] were originally generated by the W. Macklin, University of Colorado Denver Anschutz Medical Campus, Aurora, CO, and NG2-CreER^{T2} mice[24] were generated by F. Kirchhoff, Saarland University, Homburg, Germany. NG2-CreER^{T2} mice crossed to CAG-CAT-EGFP mice[25] were kindly provided by J. Ninkovic, LMU Munich, Germany. The recombinant r8-18C5-IgG anti-MOG antibody was kindly provided by K. Dornmair, LMU Munich, Germany. Some of the confocal imaging experiments were performed at the Core Facility Bioimaging of the Biomedical Center, LMU Munich (headed by S. Dietzel). This project was supported by the Deutsche Forschungsgemeinschaft (DFG), via TRR 274/1 2020 (Projects B03, C02, C05, Z01, Z02 – ID 408885537) and the Munich Center for Systems Neurology (SyNergy EXC 2145 – ID 390857198). Work in M.K.'s laboratory is further financed by the DFG (TRR128, Project B10 and B13; TRR152, Project P27), the European Research Council (ERC) under the European Union's Seventh Framework Program, FP/2007-2013, ERC grant agreement no. 310932), the German Federal Ministry of Research and Education (BMBF; Competence Network Multiple Sclerosis), the "Klaus Faber Stiftung," and the "Verein Therapieforschung für MS-Kranke e.V." T.M. was supported by the ERC under the European Union's Seventh Framework Program (FP/2007-2013; ERC grant agreement no. 616791), the German Center for Neurodegenerative Diseases (DZNE), the Hertie Foundation (P1150064), and the DFG (CRC870 A11 – ID 118803580, Mi 694/8-1 – ID 323061152, FOR ImmunoStroke A03 Mi 694/9-1 – ID 428663564). CLEM was supported via a DFG instrumentation grant (INST95/1755-1 FUGG, ID 518284373). M.K. and T.M. further received a common DFG grant (Ke 774/5-1; Mi 694/7-1). N.S.'s research is supported by a DFG research grant (ID 426715780) and instrumentation support (ID 457868227), by the Hertie Network of Excellence in Clinical Neuroscience (P1200019), and by the Else Kröner Fresenius Stiftung (2022_EKEA.162). A.M., E.M.U.G., K.E., and A.W. received support from the DFG-funded Graduate School of Systemic Neurosciences (GSC 82 – ID 24184143). M.A. was supported by SyNergy (EXC 2145, ID 390857198) and by TRR 274/1 2020, ID 408885537. N.T. was supported by the medMS Doctoral Program of the Hertie Foundation.

AUTHOR CONTRIBUTIONS

M.K. and T.M. conceived and designed the experiments. A.M., N.T., E.M.U.G., K.E., and M.A. performed *in vivo* microscopy. A.M., N.T., E.M.U.G., K.E., M.A., A.W., C.A.C., and N.S. analyzed stainings and *in vivo* recordings. N.S. and M.S. performed and analyzed correlated EM. A.M., T.M., and M.K. wrote the paper with input from all authors.

DECLARATION OF INTERESTS

The authors declare no competing interests.

Received: February 7, 2022
Revised: February 1, 2023
Accepted: March 22, 2023
Published: April 17, 2023

REFERENCES

1. Lubetzki, C., Zalc, B., Williams, A., Stadelmann, C., and Stankoff, B. (2020). Remyelination in multiple sclerosis: from basic science to clinical translation. Lancet Neurol. *19*, 678–688. https://doi.org/10.1016/S1474-4422(20)30140-X.
2. Plemel, J.R., Liu, W.Q., and Yong, V.W. (2017). Remyelination therapies: a new direction and challenge in multiple sclerosis. Nat. Rev. Drug Discov. *16*, 617–634. https://doi.org/10.1038/nrd.2017.115.
3. de Faria, O., Jr., Pivonkova, H., Varga, B., Timmler, S., Evans, K.A., and Káradóttir, R.T. (2021). Periods of synchronized myelin changes shape brain function and plasticity. Nat. Neurosci. *24*, 1508–1521. https://doi.org/10.1038/s41593-021-00917-2.
4. Franklin, R.J.M., and Ffrench-Constant, C. (2017). Regenerating CNS myelin - from mechanisms to experimental medicines. Nat. Rev. Neurosci. *18*, 753–769. https://doi.org/10.1038/nrn.2017.136.
5. Duncan, I.D., Radcliff, A.B., Heidari, M., Kidd, G., August, B.K., and Wierenga, L.A. (2018). The adult oligodendrocyte can participate in remyelination. Proc. Natl. Acad. Sci. USA *115*, E11807–E11816. https://doi.org/10.1073/pnas.1808064115.
6. Yeung, M.S.Y., Djelloul, M., Steiner, E., Bernard, S., Salehpour, M., Possnert, G., Brundin, L., and Frisén, J. (2019). Dynamics of oligodendrocyte generation in multiple sclerosis. Nature *566*, 538–542. https://doi.org/10.1038/s41586-018-0842-3.
7. Jäkel, S., Agirre, E., Mendanha Falcão, A., van Bruggen, D., Lee, K.W., Knuesel, I., Malhotra, D., Ffrench-Constant, C., Williams, A., and Castelo-Branco, G. (2019). Altered human oligodendrocyte heterogeneity in multiple sclerosis. Nature *566*, 543–547. https://doi.org/10.1038/s41586-019-0903-2.
8. Bacmeister, C.M., Barr, H.J., McClain, C.R., Thornton, M.A., Nettles, D., Welle, C.G., and Hughes, E.G. (2020). Motor learning promotes remyelination via new and surviving oligodendrocytes. Nat. Neurosci. *23*, 819–831. https://doi.org/10.1038/s41593-020-0637-3.
9. Franklin, R.J.M., Frisén, J., and Lyons, D.A. (2021). Revisiting remyelination: towards a consensus on the regeneration of CNS myelin. Semin. Cell Dev. Biol. *116*, 3–9. https://doi.org/10.1016/j.semcdb.2020.09.009.
10. Romanelli, E., Merkler, D., Mezydlo, A., Weil, M.T., Weber, M.S., Nikić, I., Potz, S., Meinl, E., Matznick, F.E., Kreutzfeldt, M., et al. (2016). Myelinosome formation represents an early stage of oligodendrocyte damage in multiple sclerosis and its animal model. Nat. Commun. *7*, 13275. https://doi.org/10.1038/ncomms13275.
11. Neely, S.A., Williamson, J.M., Klingseisen, A., Zoupi, L., Early, J.J., Williams, A., and Lyons, D.A. (2022). New oligodendrocytes exhibit more abundant and accurate myelin regeneration than those that survive demyelination. Nat. Neurosci. *25*, 415–420. https://doi.org/10.1038/s41593-021-01009-x.
12. Neumann, B., Foerster, S., Zhao, C., Bodini, B., Reich, D.S., Bergles, D.E., Káradóttir, R.T., Lubetzki, C., Lairson, L.L., Zalc, B., et al. (2020). Problems and pitfalls of identifying remyelination in multiple sclerosis. Cell Stem Cell *26*, 617–619. https://doi.org/10.1016/j.stem.2020.03.017.
13. Orthmann-Murphy, J., Call, C.L., Molina-Castro, G.C., Hsieh, Y.C., Rasband, M.N., Calabresi, P.A., and Bergles, D.E. (2020). Remyelination alters the pattern of myelin in the cerebral cortex. eLife *9*. https://doi.org/10.7554/eLife.56621.
14. Jafari, M., Schumacher, A.M., Snaidero, N., Ullrich Gavilanes, E.M., Neziraj, T., Kocsis-Jutka, V., Engels, D., Jürgens, T., Wagner, I., Weidinger, J.D.F., et al. (2021). Phagocyte-mediated synapse removal in cortical neuroinflammation is promoted by local calcium accumulation. Nat. Neurosci. *24*, 355–367. https://doi.org/10.1038/s41593-020-00780-7.
15. Bodini, B., Veronese, M., García-Lorenzo, D., Battaglini, M., Poirion, E., Chardain, A., Freeman, L., Louapre, C., Tchikviladze, M., Papeix, C., et al. (2016). Dynamic imaging of individual remyelination profiles in multiple sclerosis. Ann. Neurol. *79*, 726–738. https://doi.org/10.1002/ana.24620.

16. Hughes, E.G., Orthmann-Murphy, J.L., Langseth, A.J., and Bergles, D.E. (2018). Myelin remodeling through experience-dependent oligodendrogenesis in the adult somatosensory cortex. Nat. Neurosci. *21*, 696–706. https://doi.org/10.1038/s41593-018-0121-5.

17. Hill, R.A., Li, A.M., and Grutzendler, J. (2018). Lifelong cortical myelin plasticity and age-related degeneration in the live mammalian brain. Nat. Neurosci. *21*, 683–695. https://doi.org/10.1038/s41593-018-0120-6.

18. Snaidero, N., Schifferer, M., Mezydlo, A., Zalc, B., Kerschensteiner, M., and Misgeld, T. (2020). Myelin replacement triggered by single-cell demyelination in mouse cortex. Nat. Commun. *11*, 4901. https://doi.org/10.1038/s41467-020-18632-0.

19. Mei, F., Lehmann-Horn, K., Shen, Y.A., Rankin, K.A., Stebbins, K.J., Lorrain, D.S., Pekarek, K., A Sagan, S., Xiao, L., Teuscher, C., et al. (2016). Accelerated remyelination during inflammatory demyelination prevents axonal loss and improves functional recovery. eLife *5*. https://doi.org/10.7554/eLife.18246.

20. Neumann, B., Baror, R., Zhao, C., Segel, M., Dietmann, S., Rawji, K.S., Foerster, S., McClain, C.R., Chalut, K., van Wijngaarden, P., and Franklin, R.J.M. (2019). Metformin restores CNS remyelination capacity by rejuvenating aged stem cells. Cell Stem Cell *25*. 473–485.e8. https://doi.org/10.1016/j.stem.2019.08.015.

21. Mallon, B.S., Shick, H.E., Kidd, G.J., and Macklin, W.B. (2002). Proteolipid promoter activity distinguishes two populations of NG2-positive cells throughout neonatal cortical development. J. Neurosci. *22*, 876–885. https://doi.org/10.1523/JNEUROSCI.22-03-00876.2002.

22. Bø, L., Vedeler, C.A., Nyland, H.I., Trapp, B.D., and Mørk, S.J. (2003). Subpial demyelination in the cerebral cortex of multiple sclerosis patients. J. Neuropathol. Exp. Neurol. *62*, 723–732. https://doi.org/10.1093/jnen/62.7.723.

23. Hughes, E.G., Kang, S.H., Fukaya, M., and Bergles, D.E. (2013). Oligodendrocyte progenitors balance growth with self-repulsion to achieve homeostasis in the adult brain. Nat. Neurosci. *16*, 668–676. https://doi.org/10.1038/nn.3390.

24. Huang, W., Zhao, N., Bai, X., Karram, K., Trotter, J., Goebbels, S., Scheller, A., and Kirchhoff, F. (2014). Novel NG2-CreERT2 knock-in mice demonstrate heterogeneous differentiation potential of NG2 glia during development. Glia *62*, 896–913. https://doi.org/10.1002/glia.22648.

25. Nakamura, T., Colbert, M.C., and Robbins, J. (2006). Neural crest cells retain multipotential characteristics in the developing valves and label the cardiac conduction system. Circ. Res. *98*, 1547–1554. https://doi.org/10.1161/01.RES.0000227505.19472.69.

26. Schain, A.J., Hill, R.A., and Grutzendler, J. (2014). Label-free in vivo imaging of myelinated axons in health and disease with spectral confocal reflectance microscopy. Nat. Med. *20*, 443–449. https://doi.org/10.1038/nm.3495.

27. Bottes, S., and Jessberger, S. (2021). Live imaging of remyelination in the adult mouse corpus callosum. Proc. Natl. Acad. Sci. USA *118*. https://doi.org/10.1073/pnas.2025795118.

28. Muzumdar, M.D., Tasic, B., Miyamichi, K., Li, L., and Luo, L. (2007). A global double-fluorescent Cre reporter mouse. Genesis *45*, 593–605. https://doi.org/10.1002/dvg.20335.

29. Takai, Y., Misu, T., Kaneko, K., Chihara, N., Narikawa, K., Tsuchida, S., Nishida, H., Komori, T., Seki, M., Komatsu, T., et al. (2020). Myelin oligodendrocyte glycoprotein antibody-associated disease: an immunopathological study. Brain *143*, 1431–1446. https://doi.org/10.1093/brain/awaa102.

30. Wang, J., He, X., Meng, H., Li, Y., Dmitriev, P., Tian, F., Page, J.C., Lu, Q.R., and He, Z. (2020). Robust myelination of regenerated axons induced by combined manipulations of GPR17 and microglia. Neuron *108*. 876–886.e4. https://doi.org/10.1016/j.neuron.2020.09.016.

31. Keirstead, H.S., and Blakemore, W.F. (1997). Identification of post-mitotic oligodendrocytes incapable of remyelination within the demyelinated adult spinal cord. J. Neuropathol. Exp. Neurol. *56*, 1191–1201. https://doi.org/10.1097/00005072-199711000-00003.

32. Viganò, F., Möbius, W., Götz, M., and Dimou, L. (2013). Transplantation reveals regional differences in oligodendrocyte differentiation in the adult brain. Nat. Neurosci. *16*, 1370–1372. https://doi.org/10.1038/nn.3503.

33. Merkler, D., Ernsting, T., Kerschensteiner, M., Brück, W., and Stadelmann, C. (2006). A new focal EAE model of cortical demyelination: multiple sclerosis-like lesions with rapid resolution of inflammation and extensive remyelination. Brain *129*, 1972–1983. https://doi.org/10.1093/brain/awl135.

34. Gardner, C., Magliozzi, R., Durrenberger, P.F., Howell, O.W., Rundle, J., and Reynolds, R. (2013). Cortical grey matter demyelination can be induced by elevated pro-inflammatory cytokines in the subarachnoid space of MOG-immunized rats. Brain *136*, 3596–3608. https://doi.org/10.1093/brain/awt279.

35. Wolswijk, G. (2000). Oligodendrocyte survival, loss and birth in lesions of chronic-stage multiple sclerosis. Brain *123*, 105–115. https://doi.org/10.1093/brain/123.1.105.

36. Albert, M., Antel, J., Brück, W., and Stadelmann, C. (2007). Extensive cortical remyelination in patients with chronic multiple sclerosis. Brain Pathol. *17*, 129–138. https://doi.org/10.1111/j.1750-3639.2006.00043.x.

37. Chang, A., Staugaitis, S.M., Dutta, R., Batt, C.E., Easley, K.E., Chomyk, A.M., Yong, V.W., Fox, R.J., Kidd, G.J., and Trapp, B.D. (2012). Cortical remyelination: a new target for repair therapies in multiple sclerosis. Ann. Neurol. *72*, 918–926. https://doi.org/10.1002/ana.23693.

38. Jürgens, T., Jafari, M., Kreutzfeldt, M., Bahn, E., Brück, W., Kerschensteiner, M., and Merkler, D. (2016). Reconstruction of single cortical projection neurons reveals primary spine loss in multiple sclerosis. Brain *139*, 39–46. https://doi.org/10.1093/brain/awv353.

39. Marisca, R., Hoche, T., Agirre, E., Hoodless, L.J., Barkey, W., Auer, F., Castelo-Branco, G., and Czopka, T. (2020). Functionally distinct subgroups of oligodendrocyte precursor cells integrate neural activity and execute myelin formation. Nat. Neurosci. *23*, 363–374. https://doi.org/10.1038/s41593-019-0581-2.

40. Fard, M.K., van der Meer, F., Sánchez, P., Cantuti-Castelvetri, L., Mandad, S., Jäkel, S., Fornasiero, E.F., Schmitt, S., Ehrlich, M., Starost, L., et al. (2017). BCAS1 expression defines a population of early myelinating oligodendrocytes in multiple sclerosis lesions. Sci. Transl. Med. *9*. https://doi.org/10.1126/scitranslmed.aam7816.

41. Call, C.L., and Bergles, D.E. (2021). Cortical neurons exhibit diverse myelination patterns that scale between mouse brain regions and regenerate after demyelination. Nat. Commun. *12*, 4767. https://doi.org/10.1038/s41467-021-25035-2.

42. Bei, F., Lee, H.H.C., Liu, X., Gunner, G., Jin, H., Ma, L., Wang, C., Hou, L., Hensch, T.K., Frank, E., et al. (2016). Restoration of visual function by enhancing conduction in regenerated axons. Cell *164*, 219–232. https://doi.org/10.1016/j.cell.2015.11.036.

43. Barker, R.A., Götz, M., and Parmar, M. (2018). New approaches for brain repair-from rescue to reprogramming. Nature *557*, 329–334. https://doi.org/10.1038/s41586-018-0087-1.

44. Kay, J.N., Roeser, T., Mumm, J.S., Godinho, L., Mrejeru, A., Wong, R.O., and Baier, H. (2004). Transient requirement for ganglion cells during assembly of retinal synaptic layers. Development *131*, 1331–1342. https://doi.org/10.1242/dev.01040.

45. Linnington, C., Webb, M., and Woodhams, P.L. (1984). A novel myelin-associated glycoprotein defined by a mouse monoclonal antibody. J. Neuroimmunol. *6*, 387–396. https://doi.org/10.1016/0165-5728(84)90064-x.

46. Zolotukhin, S., Byrne, B.J., Mason, E., Zolotukhin, I., Potter, M., Chesnut, K., Summerford, C., Samulski, R.J., and Muzyczka, N. (1999). Recombinant adeno-associated virus purification using novel methods improves infectious titer and yield. Gene Ther. *6*, 973–985. https://doi.org/10.1038/sj.gt.3300938.

47. Holtmaat, A., Bonhoeffer, T., Chow, D.K., Chuckowree, J., De Paola, V., Hofer, S.B., Hübener, M., Keck, T., Knott, G., Lee, W.C., et al. (2009). Long-term, high-resolution imaging in the mouse neocortex through a chronic cranial window. Nat. Protoc. *4*, 1128–1144. https://doi.org/10.1038/nprot.2009.89.

48. Bishop, D., Nikić, I., Brinkoetter, M., Knecht, S., Potz, S., Kerschensteiner, M., and Misgeld, T. (2011). Near-infrared branding efficiently correlates light and electron microscopy. Nat. Methods *8*, 568–570. https://doi.org/10.1038/nmeth.1622.

49. Longair, M.H., Baker, D.A., and Armstrong, J.D. (2011). Simple neurite tracer: open source software for reconstruction, visualization and analysis of neuronal processes. Bioinformatics *27*, 2453–2454. https://doi.org/10.1093/bioinformatics/btr390.

50. Tripathi, R.B., Jackiewicz, M., McKenzie, I.A., Kougioumtzidou, E., Grist, M., and Richardson, W.D. (2017). Remarkable stability of myelinating oligodendrocytes in mice. Cell Rep. *21*, 316–323. https://doi.org/10.1016/j.celrep.2017.09.050.

STAR★METHODS

KEY RESOURCES TABLE

REAGENT or RESOURCE	SOURCE	IDENTIFIER
Antibodies		
Chicken a-MBP (1:250)	Invitrogen/ Thermo Fisher Scientific	Cat#PA1-10008; RRID: AB_1077024
Goat a-GFP (1:1000)	Abcam	Cat#ab6672; RRID: AB_305643
Mouse a-APC/CC1 (1:150)	Merck Millipore	Cat#OP80; RRID:AB_2057371
Rabbit a-NG2 (1:250)	Merck Millipore	Cat#AB5320; RRID:AB_11213678
Rabbit a-PDGFαR (1:200)	Cell Signaling Technology	Cat#3164; RRID:AB_2162351
Rabbit a-MBP (1:200)	DAKO	Cat#A0623; RRID:AB_2650566
Rabbit a-Olig2 (1:250)	Merck Millipore	Cat#Ab9610; RRID:AB_570666
AlexaFluor-conjugated donkey a-goat 488	Invitrogen/Thermo Fisher Scientific	Cat#A-11055; RRID:AB_2534102
AlexaFluor-conjugated donkey a-chicken 647	Jackson ImmunoResearch	Cat#703-605-155; RRID: AB_2340379
AlexaFluor-conjugated goat a-mouse 594	Invitrogen/Thermo Fisher Scientific	Cat#A32742; RRID:AB_2762825
AlexaFluor-conjugated goat a-mouse 647	Invitrogen/Thermo Fisher Scientific	Cat#A32728; RRID:AB_2633277
AlexaFluor-conjugated goat a-rabbit 594	Invitrogen/ Thermo Fisher Scientific	Cat#A32740; RRID:AB_2762824
AlexaFluor-conjugated goat a-rabbit 647	Invitrogen/ Thermo Fisher Scientific	Cat#A21244; RRID:AB_2535812
Recombinant r8-818C5-IgG antibody	Provided by K. Dornmair	N/A
Bacterial and virus strains		
M. tuberculosis H37 Ra, desiccated	BD Difco	Cat#231191
AAV-MBP:mTdTomato	This manuscript	N/A
AAV-MBP:CreER^{T2}	VectorBiolabs	Cat#VB1545
HEK293T	ATCC	Cat#ATCC-CRL-3216
Chemicals, peptides, and recombinant proteins		
MOG recombinant protein (N1-N125)	Jafari et al.[14]	N/A
Incomplete Freund's adjuvant	Sigma-Aldrich	Cat#F5506
Pertussis toxin from Bordetella pertussis	Sigma-Aldrich	Cat#P7208
Pooled human donor sample	Bavarian Red Cross	N/A
Vectashield	VectorLaboratories	Cat#H-1000-10
PEG solution	Sigma-Aldrich	Cat#25322-68-3
Benzonase	Sigma-Aldrich	Cat#E1014
Pluronic-F68	Merck Millipore	Cat#P1300
Tamoxifen	Sigma-Aldrich	Cat#T5648
Histoacryl glue	B. Braun	Cat#1050052
Dental cement (liquid)	Pala Paladur, Kulzer	Cat#64707938
Dental cement (powder)	Pala Paladur, Kulzer	Cat#64707954
recombinant mouse TNF-α	R&D Systems	Cat#l410-MT/CF
recombinant murine interferon-γ	Peprotech	Cat#315-05
Metformin hydrochloride	Merck	Cat#PHR1084
Clemastine fumarate	Tocris	Cat#1453
EM paraformaldehyde	EMS	Cat#15710
EM glutaraldehyde	EMS	Cat#16220
EM osmium tetroxide	EMS	Cat#19112
Experimental models: Organisms/strains		
Mouse: Plp:eGFP	The Jackson Laboratory	JAX: 033357; RRID:IMSR_JAX:033357
Mouse: ROSA:mT/mG	The Jackson Laboratory	JAX: 007576; RRID:IMSR_JAX:007576
Mouse: C57BL/6J	The Jackson Laboratory	JAX: 000664; RRID:IMSR_JAX:000664

(*Continued on next page*)

Continued		
REAGENT or RESOURCE	SOURCE	IDENTIFIER
Mouse: BiozziABH/RijHsd	Harlan Laboratories	N/A
Mouse: NG2-CreER ^{T2}	Huang et al.[24]	N/A
Mouse: CAG-CAT-EGFP	Nakamura et al.[25]	N/A
Oligonucleotides		
1.3kB of the MBP promoter	This manuscript	N/A
MembraneTag sequence (GAP-43)	Kay et al.[44]	N/A
Recombinant DNA		
Plasmid: AAV-MBP:mTdTomato	This manuscript	N/A
AAV-capsid, AAV1 - pDP1rs - rep2/cap1	PlasmidFactory	Cat#PF401
AAV-capsid,AAV1 – pDP2rs - rep2/cap2	PlasmidFactory	Cat#PF402
pAD-helper	This manuscript	N/A
Virus: AAV1/2-MBP:mTdTomato	This manuscript	N/A
Virus: AAV1/2-MBP:CreER^{T2}	VectorBiolabs	Cat#VB1545
Software and algorithms		
Adobe Creative Suite CS6 (Photoshop, Illustrator)	Adobe Systems	www.adobe.com/de/products/ cs6.html
Fiji; ImageJ (version v1.53c)	SciJava	https://fiji.sc
GraphPad Prism (version 7.05)	GraphPad Software	https://www.graphpad.com/scientificsoftware/prism/
IMOD (version 4.7)	Regents of the University of Colorado	https://bio3d.colorado.edu/imod/
VAST (version 1.2.1)	Laboratory of Jeff Lichtman	https://lichtman.rc.fas.harvard.edu/vast/
Olympus FluoView (FV1000)	Olympus Corporation	https://www.olympus-lifescience.com/en/laser-scanning/fv3000/
Olympus FluoView (MPE-RS)	Olympus Corporation	https://www.olympus-lifescience.com/en/laser-scanning/fvmpe-rs/
Leica Application Suite X	Leica Microsystems	https://www.leica-microsystems.com/products/microscope-software/p/leica-las-x-ls/
Other		
DAPI	Invitrogen/Thermo Fisher Scientific	Cat#D1306; RRID:AB_2629482

RESOURCE AVAILABILITY

Lead contact

Requests for further information, resources and reagents should be directed to and will be fulfilled by the lead contact, Martin Kerschensteiner (Martin.Kerschensteiner@med.uni-muenchen.de).

Materials availability

All plasmids and the viruses generated in this study are available from the Lead Contact without restriction. Reagents used in the study were of general use and from commercial sources.

Data and code availability

- All data reported in this paper will be shared by the lead contact upon request.
- This paper does not report original code.
- Any additional information required to reanalyze the data reported in this work paper is available from the Lead Contact upon request.

EXPERIMENTAL MODEL AND SUBJECT DETAILS

All animal experiments were performed in accordance with regulations of the relevant animal welfare acts and protocols approved by the respective regulatory bodies (Regierung von Oberbayern).

Genotypes and sources of transgenic mice are also listed in the key resources table. This study used adult mice (2-6 months of age at the start of the experiment) from both sexes, with an F1 background of C57BL/6 (strain designation C57BL/6J, Jackson Laboratories) and BiozziABH (BiozziABH/RijHsd, Harlan Laboratories), crossbred in our animal facilities (referred to as C57BL/6× BiozziABH) for all experiments using the c-MS model. Experiments with the anti-MOG model as well as the laser ablation experiments were performed with mice on a pure C57BL/6 background. Animals were uniformly housed under standard conditions (12h lights/dark cycle, max 5 mice/cage, autoclaved food and water supplied *ad libitum*). The cages were provided with enrichment consisting of play tunnels, nestlets to be used as nesting material and a red plastic mouse house. To assess oligodendrocytes (OLs) turnover and myelin pathology at the population level *in situ* and *in vivo*, we used PLP:eGFP×BiozziABH mice (derived from Tg(Plp1-EGFP)10Wmac/J, The Jackson Laboratory), in which the PLP promoter restricts GFP expression to oligodendrocytes.[21] To label newly differentiating oligodendrocytes we used NG2-CreER^{T2} mice[24] crossed to CAG-CAT-EGFP mice[25] as a F1 cross with BiozziABH mice. For viral labeling of single oligodendrocytes for *in vivo* analysis, either C57BL/6×BiozziABH or ROSA:mT/mGxBiozziABH (derived from Gt(ROSA) 26Sortm4(ACTB-tdTomato,-EGFP)Luo/J, The Jackson Laboratory) were used. ROSA:mT/mG is characterized by widespread expression of cell membrane-targeted TdTomato (mTdTomato); upon cell-specific Cre recombination red fluorescence is replaced by membrane-targeted eGFP (mG[28]) For the combined drugs treatment, ROSA:mT/mGxBiozziABH mice received metformin hydrochloride (Merck, cat no. PHR1084) in their drinking water (300mg kg^{-1} bodyweight per day) and daily intraperitoneal (i.p.) injections with clemastine fumarate (Tocris, cat no. 1453; 10mg kg^{-1} bodyweight per day, in PBS with 10% DMSO) starting three days after c-MS lesion induction. Treatment was continued until the last multi-photon imaging time point.

Mice were randomly assigned to experimental groups. Group sample sized were chosen based on previous studies.[10,16–18]

Pre-established exclusion criteria were used in this study. Mice were excluded when showed signs of severe neurological deficits as defined in our animal protocols or, did not show signs of clinical EAE score before cytokine injection time point (only for c-MS model). Mice with decreased cranial window quality during the longitudinal *in vivo* imaging, preventing oligodendrocyte identification and reconstruction, were excluded from the analysis. Mice or tissue showing insufficient labeling or staining, or structures showing insufficient signal to noise ratios were not analyzed.

METHOD DETAILS

Induction of the cortical MS model (c-MS model)

Cortical inflammatory lesions were induced as previously described.[14] In short, animals were immunized subcutaneously under ketamine-xylazine anaesthesia (87mg kg^{-1}+3mg kg^{-1}) with a total volume of 250µl of an emulsion containing 50µg of purified recombinant myelin oligodendrocyte glycoprotein (MOG, N1-125, expressed in E. coli) and complete Freund's adjuvant (Sigma-Aldrich, catalog no. F5506) supplemented with 10mg ml^{-1} *Mycobacterium Tuberculosis* H37Ra (BD Difco, catalog no. 231191). Immunization was repeated one week later. Additionally, pertussis toxin (200ng, Sigma-Aldrich, catalog no. P7208) was injected i.p. at day 0 and 1 for both immunizations. Animals were weighted daily and evaluated by an established EAE scoring system according to the severity of locomotor deficits likely related to white matter lesions in the spinal cord: 0 – no detectable clinical signs; 0.5 – partial tail weakness; 1 – complete tail paralysis; 1.5 – gait instability; 2 – hind limb paresis; 2.5 – hind limb paresis with partial dragging; 3 – complete hind limb paralysis; 3.5 – complete hind limb paralysis and forelimb paresis; 4 – hind and fore limb paralysis; 5 – death (score above 3.5, immediate termination criteria). Cortical lesion induction was performed on animals with a clinical score >0 under anesthesia with a combination of medetomidine–midazolam–fentanyl (MMF, 0.5mg kg^{-1}+5mg kg^{-1}+0.05mg kg^{-1}) 3 weeks after initial immunization. Mice were injected intracortically (coordinates: 1.2mm lateral, 0.6mm caudal to bregma, depth 0.8mm) with 2µl of a cytokine mix of 0.125 - 0.25 µg µl^{-1} of recombinant mouse TNF-α (R&D Systems, catalog no. l410-MT/CF) and 375 - 750U µl^{-1} of recombinant murine interferon-γ (Peprotech, catalog no. 315-05) in phosphate-buffered saline (PBS)/0.1% bovine serum albumin (BSA). After the surgery, animals were injected with 250µl of saline/glucose 5% solution for rehydration and anesthesia antagonist (naloxone, 1.2mg kg^{-1}; flumazenil 0.5mg kg^{-1}; atipamezole, 2.5mg kg^{-1}). Analgesia (buprenorphine, 0.1 mg kg^{-1}) was applied every 8-12 h on the days following surgery.

Induction of the cortical anti-MOG model

To study demyelinating cortical lesions induced by anti-myelin oligodendrocyte glycoprotein (MOG) antibodies, we used adult male and female transgenic ROSA:mT/mG mice. We induced demyelinating lesions by applying a recombinant r8-18C5-IgG anti-MOG antibody[45] (courtesy of K. Dornmair, LMU Munich) at 50 µg/ml supplemented with 20% healthy pooled human donor serum as a complement source (obtained from the 'blood bank' of the Bavarian Red Cross) every 15 minutes over 60 minutes after durotomy above the area of the cortex underneath the cranial window (see below).

Laser ablation of cortical oligodendrocytes

The laser ablation of cortical oligodendrocytes was performed in ROSA:mT/mG mice using an Olympus FV-RS microscope with a MaiTai tunable laser at 920 nm and a ×25/1.05 numerical aperture (NA) water-dipping cone objective. During the cranial window surgery (see below), the mice were injected with AAV-MBP:CreER^{T2} and then induced with tamoxifen as described below. During the ablation and the following imaging sessions, the animals were anaesthetized with isoflurane (induction at 2%; imaging at 0.8-1.5% in

humidified oxygen) and placed on the microscope imaging stage, followed by constant surveillance of the health status via MouseOx (Starr Life Science Corp). The laser ablation of 1-3 cells was performed in 1-4 areas per mouse on the first day of imaging. The laser was focused on the target cell in the somatosensory cortex (920 nm, 80–120 mW for 1s in tornado mode) to ablate the cell without causing major damage to the surrounding tissue.

Immunofluorescence staining

Animals were lethally anaesthetized with isoflurane and perfused transcardially with 15-20ml Heparin/1xPBS followed by 25ml of 4% paraformaldehyde (PFA) in 1x phosphate buffered saline (1xPBS, 0.01M) using a peristaltic pump (velocity 6mL/min). Tissue was post-fixed for 12-24 h in 4% PFA, isolated and cryoprotected in 30% sucrose for 72 h. Samples were embedded in Tissue-Tek (O.C.T. Sakura Finetek Europe B.V.), frozen down in -20°C and cut in 40μm-50μm thick coronal sections on a cryostat (Leica, CM1950). A free-floating staining method was used to visualize selected markers. Sections were rinsed with 1xPBS at room temperature and blocked for 1 h with 10% goat serum (GS) or horse serum (HS) in 0.5% Triton X-100/1xPBS. An antigen retrieval step was necessary to unmask epitopes recognized by anti-NG2 and anti-PDGFαR. Sections were therefore treated with pre-heated 10mM sodium citrate buffer pH 8.5 for 25 min at 85°C and further rinsed with 1xPBS before proceeding to the blocking step. Methanol treatment was needed to obtain crisp MBP staining. Sections were incubated in cold methanol for 10-20 min at -20°C and further rinsed with 1xPBS before proceeding to the blocking step. Sections were incubated overnight at 4°C (shaking) with the following primary antibodies: mouse anti-APC/CC1 (1:150, Merck Millipore, catalog no. OP80); rabbit anti-NeuN (1:400, Sigma Aldrich, catalog no. SAB4300883); rabbit anti-NG2 (1:250, Merck Millipore, catalog no. AB5320); rabbit anti-PDGFαR (1:200, Cell Signaling Tech, catalog no. 3164); rabbit anti-MBP (1:200, DAKO, catalog no. A0623); chicken anti-MBP (1:250, Thermofisher, catalog no. PA1-10008); rabbit anti-Olig2 (1:250, Merck Millipore, catalog no. Ab9610); goat anti-GFP (1:1000, Abcam, catalog no. ab6673) in 1% GS or HS in 0.5% Triton X-100/1xPBS. Sections were washed with 1xPBS and incubated overnight at 4°C with AlexaFluor-conjugated goat anti-mouse 594 (Invitrogen, catalog no. A32742); AlexaFluor-conjugated goat anti-mouse 647 (Invitrogen, catalog no. A32728); AlexaFluor-conjugated goat anti-rabbit 594 (Invitrogen, catalog no. A32740); AlexaFluor-conjugated goat anti-rabbit 647 (Invitrogen, catalog no. A21244) antibodies (all diluted 1:1000) as well as AlexaFluor-conjugated donkey anti-rabbit 405 (Abcam, catalog no. ab175651); AlexaFluor-conjugated donkey anti-chicken 647 (Jackson Immunoresearch, catalog no. 703-605-155); AlexaFluor-conjugated donkey anti-goat 488 (Invitrogen, catalog no. A-11055) (all diluted 1:500). Samples were counterstained with DAPI (1:10 000, Invitrogen, catalog no. 62247; except for section stained for NeuN and MBP) and later mounted with Vectashield (VectorLaboratories, catalog no. H-1000-10).

Confocal microscopy

Sections with fluorescence labeling were imaged with an upright Olympus FV1000 confocal microscope equipped with x10/0.4 air, x20/0.85 oil and x60/1.42 oil immersion objectives. To demonstrate the extent of myelin damage in the cortical gray matter lesions in PLP:eGFPxBiozziABH, low magnification images were taken with x20/0.85 oil objective, z-spacing 1.5μm and pixel resolution 2.5μm pixel^{-1}. To characterize oligodendrocyte populations, define oligodendrocyte number and assess myelin recovery in cortical gray matter of PLP:eGFPxBiozziABH mice, as well as to characterize mGFP+ cells and MBP density in ROSA:mT/mGxBiozziABH mice, high magnification images were taken with a x60/1.42 oil objective, z-spacing 0.33μm and pixel resolution 0.27μm pixel^{-1}. Sections with fluorescence labeling for MBP and NeuN were imaged with an upright Leica SP8X WLL confocal microscope, equipped with a 405 nm laser, WLL2 laser (470-670 nm) and acusto-optical beam splitter. To assess myelin wrapping lower magnification images were acquired with a x20/0.75 CS2 oil immersion objective, z-spacing 1 μm and resolution 0.27μm pixel^{-1}. The following fluorescence setting were used: for NeuN with AlexaFluor 405 (excitation 405; emission 415-457), MBP with AlexaFluor 647 (excitation 647; emission 661-703 nm). NeuN and MBP were recorded with hybrid photo detectors (HyDs). For evaluation of MBP labeling of internodes formed by newly differentiating oligodendrocytes, sections with fluorescence labeling for MBP and GFP were imaged with an upright Leica SP8 confocal microscope, equipped with standard filter sets and laser lines. Images were acquired with a x40/1.30 CS2 oil immersion objective, z-spacing 0.5μm and pixel size 0.14 pixel^{-1}.

All images were processed with ImageJ or Adobe Photoshop software.

To confirm the myelination status of putative internodes derived from newly differentiated oligodendrocyte, NG2-CreER^{T2}xCAG-CAT-EGFPxBiozziABH mice were transcardially perfused with 4% PFA after two photon *in vivo* imaging. To visualize myelination of newly formed internodes, cortical regions previously imaged *in vivo* were identified and imaged through the pre-existing cranial window. Imaging was performed on a Leica SP8 MP upright microscope equipped with a multiphoton (MP) InSight DS+ Single laser (Spectra Physics) and one-photon excitation lasers at wavelengths 488, 552 and 638nm. Images were recorded using an HC IRAPO L x25/1.00 W motCORR objective; z-spacing 0.50μm, pixel resolution 0.22μm pixel^{-1}. NG2:eGFP was excited using the two-photon laser at 940nm, followed by spectral confocal reflectance (SCoRe) microscopy using all 3 one-photon excitation lasers mentioned above. Detector settings were based on settings previously described[26] at a 5nm range around the excitation wavelength. Laser lines used for SCoRe: 458, 561, 633nm, with respective detector ranges: 456-461, 559-564, 631-636nm. Additional investigation of myelination was performed on 50μm tissue slices stained with an MBP antibody as described above. Imaging was performed on a Leica SP8, equipped with standard filter sets and laser lines, using a x40/1.30 CS2 oil immersion objective; z-spacing 0.50μm, pixel resolution 0.19μm pixel^{-1}. All images were processed with ImageJ.

AAV vector generation and virus production

An AAV-MBP:mTdTomato virus was produced as previously described.[18] Briefly, the first 1.3 kb of the MBP promoter was inserted in the backbone, containing a targeting sequence, which guides the tdTomato to the plasma membrane[44] (pAAV-MBP:mTdTomato). AAV vector packaging was performed using human embryonic kidney 293 (HEK 293) cells as described before.[46] In short, HEK 293 cells were transfected with a pAD-helper, AAV-capsid (AAV1, PlasmidFactory, pDP1rs - rep2/cap1), and AAV-construct (molar ratio 3:2:5) using the RPMI:PEI incubation protocol. The AAV vector was harvested from the supernatant (with PEG solution, Sigma-Aldrich, catalog no. 25322-68-3) and the pellet. Freeze/thaw cycles were utilized to lyse the cells. Any residual DNA from the packaging process was degraded with benzonase (Sigma-Aldrich, catalog no. E1014) before proceeding to the purification step. Virus was purified using iodixanol gradient ultracentrifugation and concentrated by subsequent incubation/centrifugation with formulation buffer (Pluronic-F68 0.001%, Merck, catalog no. P1300). We obtained ~300µl of the virus, which was stored in small aliquots at -80°C. Genomic titers were ~2.5×10^{13}.

AAV-MBP:CreER^{T2} virus was purchased from VectorBiolabs (catalog no. VB1545) to induce specific GFP-labeling of surviving oligodendrocytes in ROSA:mT/mGxBiozziABH and ROSA:mT/mG mice.

Single-cell labeling of individual oligodendrocytes

For sparse virus labeling of oligodendrocytes, 1µl of the AAV-MBP:mTdTomato virus was stereotactically injected into the somatosensory cortex (coordinates - 2mm lateral, 2mm caudal to bregma, depth 0.1-0.2mm, titer 2.5×10^{13}) of C57BL/6×BiozziABH mice. Animals received a single, intracerebral injection at the day of initial immunization or 21 days before the first imaging session in control (non-immunized, cytokine injected) animals. For specific virus labeling of surviving oligodendrocytes in the c-MS model, 0.5µl of the AAV-MBP:CreER^{T2} virus was stereotactically injected into the somatosensory cortex (coordinates - 2 mm lateral, 2 mm caudal to bregma, depth 0.1-0.2 mm, titer 3.0×10^{13}) of ROSA:mT/mGxBiozziABH mice. Animals received a single, intracerebral injection 35 days before initial immunization or 56 days before the first imaging session in control (non-immunized, cytokine injected) animals. To induce expression of mGFP, animals were injected intraperitoneally with tamoxifen (75mg kg^{-1} in corn oil, Sigma-Aldrich, catalog no. T5648) once every 24 h for a total of 4 consecutive days, starting 12 days after viral injection. Some astrocytes appeared to be labeled as well with this approach and were used as additional fiducial marks. In rare cases new labeled oligodendrocytes appeared between imaging time points; if this was observed these regions were excluded from analysis.

To induce labeling of surviving oligodendrocytes in the anti-MOG model or in the laser ablation model ROSA:mT/mG mice were injected intracerebrally (0.3µm depth, right primary somatosensory cortex) with AAV-MBP:CreER^{T2} 35 days or 46 days, respectively before induction and the first imaging session. To induce expression of mGFP, animals were injected i.p. with tamoxifen as described above starting 14 days after viral injection.

Cranial window surgery

To gain optical access to the cortex, we performed a craniotomy and implanted a cranial window above the somatosensory cortex of PLP:eGFPxBiozziABH, C57BL/6×BiozziABH (injected with AAV-MBP:mTdTomato) and ROSA:mT/mGxBiozziABH or ROSA:mT/mG (both injected with AAV-MBP:CreER^{T2}) mice as previously described.[47] The cranial window was implanted on the day of the first *in vivo* imaging session or on the day of the virus injection (for the laser ablation experiments). In short, animals anesthetized with medetomidine–midazolam–fentanyl (MMF, 0.5mg kg^{-1}+5mg kg^{-1}+0.05mg kg^{-1}) were head-fixed in the stereotaxic frame and the skin was disinfected. Craniotomy was performed with a 0.5mm stainless steel drill head (Meisinger), and the bone replaced with a Ø 4mm cover glass, which was sealed using histoacryl glue (B. Braun, catalog no. 1050052) and dental cement (Pala Paladur, Kulzer, catalog no. 64707954 (powder) and 64707938 (liquid)). After the surgery, animals were injected with 250µl of saline/glucose 5% solution for rehydration and the anesthesia was antagonized (naloxone, 1.2mg kg^{-1}; flumazenil 0.5mg kg^{-1}; atipamezole, 2.5mg kg^{-1}). Analgesia (buprenorphine, 0.1mg kg^{-1}) was applied every 8-12 h on the days following surgery.

In vivo imaging

For chronic longitudinal *in vivo* imaging of oligodendrocytes and myelin recovery in cortical lesions, cranial windows were implanted on the day of first imaging session as described above. To investigate oligodendrocyte turnover and proximal process formation, the same areas were imaged 3 days after c-MS induction and in the recovery phase (day 14 to 16 after c-MS induction, referred to as 'c-MS d3/14/16', respectively, throughout the manuscript). In a subset of experiments, additional imaging was performed at c-MS day 25 to document longer term outcomes. In parallel, control (non-immunized) animals were imaged before cytokine injection (baseline), as well as 3 and 14 days after the cytokine injection. During an imaging session, animals were anaesthetized with medetomidine–midazolam–fentanyl (MMF, 0.5mg kg^{-1}+5mg kg^{-1}+0.05mg kg^{-1}) and placed on the microscope imaging stage with a custom-designed head-fixing device. Imaging was performed on 3 to 5 areas of interest located in layer 1 of somatosensory cortex at 15Hz with an Olympus MPE-RS multi-photon system using a resonant scanner and a femto-second pulsed Ti:Sapphire laser (tuned at 840nm for eGFP in PLP:eGFPxBiozziABH, 1040nm for viral-induced expression of mTdTomato and 820nm for Cre recombinase-mediated expression of mGFP in oligodendrocytes and their internodes) with a maximum power of 20mW (measured at the back focal plan) using a 25x/1.25 water-immersion Olympus objective; z-spacing 0.50µm, pixel resolution 0.17µm pixel^{-1}, dwell time 4µs. After each imaging session, animals were injected with 250µl of saline/glucose 5% solution for rehydration and anesthesia was antagonized (naloxone, 1.2mg kg^{-1}; flumazenil 0.5mg kg^{-1}; atipamezole, 2.5mg kg^{-1}).

To monitor surviving oligodendrocytes in the anti-MOG model, we performed chronic longitudinal *in vivo* imaging of the same imaging areas as described above starting right before the lesion induction, on day 7 after cortical anti-MOG lesion induction and in the recovery phase, at day 18. Imaging of the same areas was performed with resonant scanner, 16x averaging, pixel size of 0.33 μm in x/y and 0.5 μm in z (baseline imaging before lesion induction) or with galvanometric mirrors using no averaging, a pixel size of 0.25 μm in x/y in z (subsequent imaging at day 7 and day 18).

To investigate the formation and lateral extension of internodes derived from surviving oligodendrocytes, following laser ablation, ROSA:mT/mG mice were imaged at the day of laser ablation (day 0) and weekly until day 58. For the analysis only the time points before laser ablation (day 0), the time point at which oligodendrocyte cell loss was confirmed (day 7), a time point at which most of the myelin was lost (day 29) and a time point at which remyelination is expected to be advanced (day 58[18]) were used. The longitudinal *in vivo* imaging of the same areas was performed using an Olympus FV-RS microscope with a tunable laser at 920 nm and a 25x/1.05 numerical aperture (NA) water-dipping cone objective. Images were acquired with resonant scanner, 16x averaging, pixel size of 0.33 μm in x/y and 0.5 μm in z. The final imaging at day 72 was performed on the FV1000 MPE with a x25/1.05 numerical aperture (NA) water-dipping cone objective. The two-photon *in vivo* imaging was performed with a wavelength of 910 nm, a pixel size of 0.38 μm in x/y and 0.5 μm in z. Additionally, SCoRe was performed using 488, 559 and 635-nm laser wavelength outputs using a 20/80 beamsplitter. Reflected light was detected using three photodetectors using suitable dichroic mirrors and band pass filters centered on the laser wavelengths (486–491 nm, 557–562 nm and 632–640 nm).

Mice were sacrificed after the last imaging session. Animals with decreased cranial window quality throughout the imaging course or with excessive OL depletion (in the case of the anti-MOG model) were excluded from analysis. No signs of phototoxicity (such as cell membrane blebbing or cell death) were observed in control animals.

Correlative light-to-electron microscopy (CLEM)

C57BL/6×BiozziABH mice, injected with AAV-MBP:mTdTomato, were lethally anesthetized with isoflurane and perfused transcardially with 5ml HBSS followed by 30ml of EM-fixative (2.5% glutaraldehyde, 4% paraformaldehyde in 1xPBS) using a peristaltic pump. Tissue was extracted and post-fixed for 8 h at 4°C in EM-fixative. After post-fixation, brains were positioned back under the two-photon microscope, so the area of interest could be re-identified. Asymmetric near-infrared branding marks (NIRB[48]) were placed around the previously imaged area in order to enable further identification of specific oligodendrocytes with electron microscopy (EM). Tissue was sequentially treated with 2% osmium tetroxide (EMS) in sodium cacodylate buffer pH 7.4 followed by 1.5% potassium ferricyanide in the same buffer. Each treatment lasted for 2x45 min. Once dehydrated using ethanol and infiltrated with LX112, samples were sectioned on the ATUMtome (Powertome, RMC). Consecutive 50nm thick sections were generated with a 35° ultra-diamond knife and collected on plasma-treated, carbon-coated Kapton tape (kindly provided by Jeff Lichtman, Harvard University). EM images of larger, pre-defined area of interest (based on venous architecture and NIRB marks) were obtained on a Zeiss Crossbeam Gemini 340 SEM with a four-quadrant backscattered electron detector at 8kV. At first, overview low-resolution images (5000nm pixel^{-1}) were taken to more precisely define the area of interest. Then, a smaller selected region was imaged at 200 x 200nm^2 and after additional selection, a final region of interest was imaged at 50x50nm^2. EM image stacks were aligned by automatic and manual processing in ImageJ (Fiji) TrakEM. 3-D reconstructions were processed in IMOD (version 4.7) and VAST (version 1.2.1) software packages.

QUANTIFICATION AND STATISTICAL ANALYSIS

Image processing and analysis

Data collection and analysis was performed blind to the conditions of the experiment, unless this was not possible due to the longitudinal nature of the imaging and/or an obvious disease phenotype.

Post-processing of presented confocal and multiphoton microscopes images was done using the open-source image analysis software ImageJ (Fiji) and Photoshop (Adobe). Further image processing steps are stated in the text or figure legends.

To analyze oligodendrocyte number and myelin length at the population level, PLP:eGFPxBiozziABH mice were perfused with 4% 1xPFA at c-MS day 3 and c-MS day 14 and age-matched healthy (non-immunized) mice were used as controls. Coronal sections of the brain were cut (±200 μm anterior/posterior from the injection site) and stained with anti-MBP (myelin)/anti-CC1 (mature oligodendrocytes)/anti-NG2 (OPCs)/anti-PDGFαR (OPCs)/anti-Olig2 (oligodendrocyte lineage) antibody and DAPI as described above. For each animal, three regions of cortical layer 1 and 2/3 were imaged ~300μm laterally to the injection site. ImageJ (Fiji) plugins were used for processing and quantification: the 'cell counter' to count oligodendrocyte number (PLP:eGFP) as well as the CC1, NG2, PDGFαR, Olig2 positive cells; the 'freehand line tracing tool' to mark and measure the length of the internodes (MBP) positioned within three squares defined by the ImageJ (Fiji) 'grid' plugin (area per point 5000 μm^2; 33% of the total area, tracing every 15 frames of stacks with ~120 frames). To assess oligodendrocyte turnover and oligodendrocyte process length *in vivo*, PLP:eGFPxBiozziABH mice were imaged at the c-MS day 3 and c-MS day 16. Two photon image stacks were processed with ImageJ (Fiji) to adjust brightness and contrast. Oligodendrocytes were compared between time points and marked with 'cell counter' as '*remain*' for the ones that stayed over time; '*lost*' which were present at day 3 and not detected at day 16; '*new*', which were only present at the day 16 and not day 3. Total oligodendrocyte process length was marked and measured with the 'freehand line tracing' tool at both time points, as

described above for *in situ* analysis. Reconstructions of processes and internodes in Figure 1G (c-MS day 3 and c-MS day 16) are based on PLP:eGFPxBiozziABH maximum intensity projections of the corresponding imaging time points.

To investigate proximal process formation of surviving oligodendrocytes, C57BL/6×BiozziABH mice (injected with the AAV-MBP:mTdTomato) were imaged at c-MS day 3 and c-MS day 16. Two-photon images were processed with ImageJ (Fiji) and oligodendrocytes were selected for further single cell reconstruction with the 'simple neurite tracing' plugin.[49] When comparing two time points (c-MS day 3, c-MS day 16) the numbers of all, lost and new oligodendrocyte proximal processes (per individual oligodendrocyte) were counted. In 'proximal process' quantifications we included the primary processes emerging from the soma, as well as their branches in the immediate vicinity of the soma, which can be difficult to disambiguate from primary processes. Moreover, further oligodendrocyte processes and internodes were also reconstructed when comparing three time points (pre c-MS, c-MS day 3, c-MS day 16); starting with primary processes until reaching the connected internode. Reconstructions based on the two-photon data were used in CLEM. Age-matched but non-immunized AAV-MBP:mTdTomato- and cytokine-injected controls were imaged at the same time points as the experimental animals.

For the correlated 3D EM reconstructions, EM images were aligned by a sequence of automatic and manual processing steps in Fiji TrakEM and IMOD software was then used for manual segmentation, tracing, and reconstructions of the CLEM volumes.

To analyze differentiation and internode formation of newly differentiated oligodendrocytes, NG2-CreER^{T2}xCAG-CAT-EGFPx-BiozziABH mice were imaged at pre c-MS, c-MS day 3, c-MS day 16 and c-MS day 25. Two-photon images were processed with ImageJ (Fiji) and imaged areas were selected for analysis by image quality. Different time points of the same areas were analyzed side by side. The identity of GFP+ cells was visually determined by morphology of the soma and presence of internodes for each imaging area and counted using the 'cell counter' plugin. For the cell density analysis all GFP+ cells were counted and normalized to the cell density in this area at the pre c-MS time point. For the analysis of GFP+ oligodendrocytes only those GFP+ cells that connected to internodes were counted and related to the volume of the imaged stack. For the analysis of added internodes, only 'newly differentiating oligodendrocytes' were included. These were defined as cells that showed an OPC morphology (and did not connect to internodes) at the pre-cMS time point and then extended putative internodes at any time point thereafter. The few GFP+ cells that already extended internodes at the pre c-MS time point were not included in this analysis. Internode segments of oligodendrocytes were reconstructed using the ''simple neurite tracing'' plugin in ImageJ (Fiji). Respective values of the traces were manipulated in R.

To analyze internode formation of surviving oligodendrocytes, ROSA:mT/mGxBiozziABH animals were injected with AAV-MBP:CreER^{T2,} and mGFP expression was induced by tamoxifen administration as described above. Mice were imaged before cortical lesion induction and at c-MS day 3, day 16 and in some cases day 25. To quantify the total length of internodes, as well as to assess the lost, new and remaining internodes in surviving oligodendrocytes, 3D reconstructions of all myelin segments were performed within the acquired chronic *in vivo* imaging volumes (oligodendrocyte number/volume = 1-4) using the 'simple neurite tracing' plugin in ImageJ (Fiji). The total number of internodes and their individual length were measured and related to the number of oligodendrocytes per imaged area to calculate the total internode length and internode number per oligodendrocyte. To track the individual fate of internodes we compared the internode reconstructions between the c-MS time points. Internodes were marked as '*remain*' for the ones that stayed over the course of c-MS and did not experience any length changes; '*lost*' which were present before c-MS induction and not detectable at the latest imaging time point and '*shortened*' if their length decreased by at least 10 μm between two imaging time points. The internode length removed due to shortened and lost internodes per oligodendrocyte was related the total internode length of the oligodendrocyte at the pre c-MS time point to calculate the ''proportion of internode loss [% of pre]''.

Internodes were classified as '*newly formed*' when they were only present at the c-MS day 16 or day 25 time point but were not present at the preceding imaging session. Internodes were classified as '*extended*' internodes if they had increased their length between two imaging time points by more than 10 μm. The internode length gained due to extended and newly formed internodes per oligodendrocyte was related the total internode length of the oligodendrocyte at the pre c-MS time point to calculate the ''proportion of internode gain [% of pre]''. Further for extended or newly formed internodes we determined whether they '*restored*' myelination on a previously demyelinated segment i.e. a segment that at the pre c-MS time point was myelinated by a labeled mature oligodendrocyte or whether they '*de novo*' provided myelination to a segment that was not previously myelinated by any labeled surviving oligodendrocyte.

To analyze internode damage, internode swellings were counted with the 'point tool' in base ImageJ (Fiji) and assigned to their corresponding internode, which were previously analyzed with the 'simple neurite tracing' plugin in ImageJ (Fiji).

To investigate the frequency of myelin wrapping around neuronal cell bodies *in situ*, mice were perfused with 4% 1xPFA at c-MS day 3 and c-MS day 14 and age-matched healthy (not immunized) mice were used as controls. Fixed tissue was cut into 50 μm coronal sections (±200 μm anterior/posterior from the injection site) and stained with anti-MBP (myelin) and NeuN as described above. For each animal, an area of cortex ipsi- and contralateral to the injection site was imaged spanning all 6 cortical layers (positioned ~200μm laterally to the injection site or at the corresponding position in the contralateral hemisphere). Images were converted to Imaris files and subsequently per mouse 10 images (5 each from the ipsilateral and contralateral hemispheres) were analyzed. First brightness and contrast were adjusted. The spots function was used with a 15μm diameter and a threshold of 1.6-2.7 to reconstruct NeuN+ nuclei as a measure of neuron number. The NeuN channel was further used to define the border between layers. The MBP channel was used to look for wrappings around cell bodies, defined as follows: (1) a spherical myelin (MBP+) structure with a NeuN positive center that (2) is derived from a single myelin internode, (3) is closed on all sides and that (4) persists for at least 3 z-slices.

To analyze myelin wrapping around neuronal cell bodies derived from surviving oligodendrocytes, ROSAmT/mGxBiozziABH mice were perfused at c-MS day 25 with 4% 1xPFA. Fixed tissue was cut into 50 μm coronal sections (±200 μm anterior/posterior from the injection site) and stained with anti-MBP (myelin) and DAPI as described above. For each animal, three regions of cortical layer 1 and 2/3 were imaged ∼300μm laterally to the injection site. In ImageJ (Fiji), the 'cell counter' plugin was used to count oligodendrocyte numbers. The DAPI channel was used to define the border between layer 1 and layer 2/3, while GFP and MBP channels were used together to look for wrappings around cell bodies, defined as follows: (1) spherical GFP+ myelin (MBP+) structure with a DAPI positive center that (2) originates from a single internode, (3) is closed on all sides and (4) persists for at least 3 z-slices.

In the cortical anti-MOG model we evaluated the formation of new internodes and quantified oligodendrocyte cell numbers in the same longitudinally imaged areas before lesion induction, in the acute phase (day 7) and in the recovery phase (day 18) of the model. As described above, we processed images with ImageJ (Fiji) and the 'simple neurite tracing' plugin[49] for internode tracing and oligodendrocyte numbers.

To investigate the formation and lateral extension of internodes derived from surviving oligodendrocytes after laser ablation of their neighbors, longitudinal *in vivo* imaging was performed as described above. The image stacks were then processed with ImageJ (Fiji) to adjust brightness and contrast. Reconstructions of internodes were done with the 'simple neurite tracing' plugin.[49] All internodes that were lost after the oligodendrocyte ablation were reconstructed while comparing two time points (day 0, day 29). Furthermore, the time points days 0, 29 and 58 were compared to identify possible internode formation of surviving oligodendrocytes. To determine a potential lateral growth, internodes neighboring the later lost internodes were reconstructed at days 0, 29 and 58 to compare their length. Surviving oligodendrocytes after the ablation at day 0 were labeled with 'cell counter' in all three time points (day 0, day 29, day 58) and compared. The ones who had a neighborhood relationship with the ablation zone were defined by a proximity of below 75 μm to the ablated cells (as the span of an oligodendrocyte is about 150 μm[50]).

Quantification of MBP+ and SCoRe+ internodes derived from newly differentiating oligodendrocytes was performed on tissue from NG2-CreER^{T2}xCAG-CAT-EGFPXBiozziABH mice perfused at c-MS day 16 with 4% 1xPFA. Tissue was postfixed for 24h and stained with MBP as described above (sections of 50μm thickness, area under cranial window used for two-photon imaging). Internodes were traced based on NG2:eGFP signal using the ''simple neurite tracer'' Fiji plugin and checked for overlapping MBP and/or SCoRe signal.

To characterize mGFP+ oligodendrocytes in ROSA:mT/mGxBiozziABH (injected with AAV-MBP:CreER^{T2,} and induced by tamoxifen as described above), animals were perfused with 4% PFA, and coronal sections of the brain were cut (±100μm anterior/posterior from the viral injection site) and stained with anti-CC1 (mature oligodendrocytes)/ anti-PDGFαR (OPCs)/ anti-Olig2 (oligodendrocyte lineage) antibodies and DAPI as described above. For each animal, three examples of cortical regions were imaged. The ImageJ (Fiji) 'cell counter' plugin was used for processing and quantification of CC1, PDGFαR, Olig2 positive cells with an overlay of mGFP+ signal.

Statistical analysis

Statistical details of experiments, including statistical test used and level of statistical significance can be found in the figure legends with number of animals/areas/oligodendrocytes per group. Sample sizes were chosen according to previous *in vivo* imaging studies of oligodendrocytes.[10,16–18,36] Microsoft Excel software was used for data compilation. Results are given as mean ± SEM. Statistical significance was analyzed with GraphPad Prism 7.0. For samples where normal distribution could be confirmed with the Pearson test the following tests were used: for two samples comparison, t test; for more than 2 samples, one-way ANOVA followed by Tukey's multiple comparison test. In non-normally distributed samples we used: for two samples comparison, nonparametric Mann-Whitney U test; for more than 2 samples Kruskal-Wallis followed by Dunn's multiple comparison test. Averages denoted in figures represent means, with error bars representing the standard error of the means. Obtained p values were stated as significance levels in the figure legends and marked in the graphs by asterisks (****$p < 0.0001$, ***$p < 0.001$; **$p < 0.01$; *$p < 0.05$).